



January 2020

Feasibility Of Downscaling NAAPS Aerosol Fields For Incorporating More Realistic Aerosol Direct Effects In WRF-Chem Simulations

Brittany Nikole Carson

Follow this and additional works at: <https://commons.und.edu/theses>

Recommended Citation

Carson, Brittany Nikole, "Feasibility Of Downscaling NAAPS Aerosol Fields For Incorporating More Realistic Aerosol Direct Effects In WRF-Chem Simulations" (2020). *Theses and Dissertations*. 3261. <https://commons.und.edu/theses/3261>

This Thesis is brought to you for free and open access by the Theses, Dissertations, and Senior Projects at UND Scholarly Commons. It has been accepted for inclusion in Theses and Dissertations by an authorized administrator of UND Scholarly Commons. For more information, please contact und.common@library.und.edu.

FEASIBILITY OF DOWNSCALING NAAPS AEROSOL FIELDS
FOR INCORPORATING MORE REALISTIC AEROSOL DIRECT
EFFECTS IN WRF-CHEM SIMULATIONS

by

Brittany Nikole Carson
Bachelor of Science, University of Louisiana Monroe, 2013

A Thesis

Submitted to the Graduate Faculty

of the

University of North Dakota

in partial fulfillment of the requirements

for the degree of

Master of Science

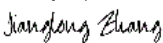
Grand Forks, North Dakota

August


2020

Copyright 2020 Brittany N. Carson

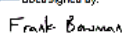
This thesis _____, submitted by Brittany Carson _____ in partial fulfillment of the requirements for the Degree of Master of Science in Atmospheric Sciences from the University of North Dakota, has been read by the Faculty Advisory Committee under whom the work has been done and is hereby approved.

DocuSigned by:


Dr. Jianglong Zhang

DocuSigned by:


Dr. Aaron Kennedy

DocuSigned by:


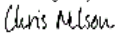
Dr. Frank Bowman

Name of Committee Member 3

Name of Committee Member 4

Name of Committee Member 5

This thesis _____ is being submitted by the appointed advisory committee as having met all of the requirements of the School of Graduate Studies at the University of North Dakota and is hereby approved.

DocuSigned by:


Chris Nelson
Dean of the School of Graduate Studies

4/8/2020

Date

PERMISSION

Title: Feasibility of Downscaling NAAPS Aerosol Fields for
Incorporating More Realistic Aerosol Direct Effects in
WRF-Chem Simulations

Department: Atmospheric Sciences

Degree: Master of Science

In presenting this thesis in partial fulfillment of the requirements for a graduate degree from the University of North Dakota, I agree that the library of this University shall make it freely available for inspection. I further agree that permission for extensive copying for scholarly purposes may be granted by the professor who supervised my thesis work or, in his absence, by the Chairperson of the department or the dean of the School of Graduate Studies. It is understood that any copying or publication or other use of this thesis or part thereof for financial gain shall not be allowed without my written permission. It is also understood that due recognition shall be given to me and to the University of North Dakota in any scholarly use which may be made of any material in my dissertation.

Brittany Nikole Carson
August 2020

TABLE OF CONTENTS

LIST OF FIGURES	vii
LIST OF TABLES	x
ACKNOWLEDGMENTS	xi
ABSTRACT	xiii
CHAPTER	
1 INTRODUCTION	1
2 BACKGROUND	5
3 MODELS AND DATASETS	11
3.1 WRF-Chem	11
3.2 Navy Aerosol Analysis and Prediction System (NAAPS) . .	14
3.3 North American Mesoscale (NAM) Analyses and Forecasts	16
3.4 Automated Surface Observing System (ASOS) and North Dakota Agricultural Weather Network (NDAWN) Data . .	17
3.5 Aerosol Robotic Network (AERONET) Data	18
4 METHODS	20
4.1 Experimental Design	20
4.1.1 Modification of WRF-Chem Initial Conditions for Aerosols	21
4.1.2 Modification of WRF-Chem Boundary Conditions for Aerosols	22
4.2 Aerosol Optical Depth Calculation	25
4.3 Evaluation Methods	26
5 RESULTS AND DISCUSSIONS	28
5.1 Aerosol Optical Depth Analysis	28
5.2 Impacts to Surface Downward Shortwave Radiation	31

5.3	Impacts to Surface Temperature	35
5.4	Impacts to 10m Wind Speeds	39
5.5	Impacts to Planetary Boundary Layer Height	41
5.6	Forecast Sensitivity Study	44
6	CONCLUSIONS	53
	REFERENCES	56

LIST OF FIGURES

Figure	Page	
1	NASA Worldview Aqua MODIS visible imagery for (a) 20:25 UTC on 28 June, (b) 19:30 UTC on 29 June, and (c) 20:15 UTC on 30 June 2015. From NASA Worldview	6
2	ECMWF Reanalysis of 700 hPa geopotential heights overlaid on winds for (a) 28 June, (b) 29 June, and (c) 30 June 2015 at 18Z. From Zhang et al., 2016	8
3	A time series of forecasted maximum temperature for 29 June 2015 at Bismarck (blue) and Grand Forks (red) National Weather Service offices. Observed maximum temperatures for 29 June are indicated by the short lines on right-hand side of plot at each NWS office. From Zhang et al., 2016.	9
4	Depiction of the WRF-Chem model domain used in this study. Yellow circles represent ASOS stations and pink triangles represent NDAWN stations used in this study	12
5	Image of the AERONET site located in Grand Forks, ND. Photo from Grand Forks, ND AERONET website by NASA (https://aeronet.gsfc.nasa.gov/new_web/photo_db_v3/Grand_Forks.html).	19
6	Flow chart representing the basic steps for running WRF-Chem with and without NAAPS data. The black outlined box includes extra steps necessary for including NAAPS aerosol data in WRF-Chem modeling.	21
7	The four boundaries can be seen in this figure. The inner domain is colored in green. The boundary width is comprised of both the yellow specified rows/columns and blue relaxation rows/columns. Figure is from Skamarock et al. (2008).	24

8	<p>(a), (b), (c) Spatial distributions of NAAPS total column AOD spatial plots for the WRF-Chem domain for 28 Jun 2015 at 00Z, 29 Jun at 15Z, and 29 Jun at 18Z, respectively. (d), (e), (f) as in (a), (b), (c) but for WRF-Chem simulated total column AOD from the chemistry run.</p>	29
9	<p>(a) Aqua MODIS imagery for 29 June 2015 at ~19:30 UTC. (b) as (a) but with overlaid AOD values. Yellows indicate lower AODs (less than 1.0) while reds indicate higher (greater than 1.0). Unshaded areas indicate regions without aerosol or thick smoke plumes that are misclassified as cloud by the MODIS aerosol retrieval algorithm. From NASA Worldview.</p>	30
10	<p>(a) SW flux for 29 June at 18Z from the WRF-Chem control simulation. (b) as in (a) but for WRF-Chem chemistry simulation. (c) Difference in SW flux between WRF-Chem chemistry and control runs where reds indicate more SW reaching the surface in Chemistry run and blues indicate less SW reaching the surface in the Chemistry run compared to Control. (d) AODs from WRF-Chem chemistry run for 29 June at 18Z. (e) Differences in SW flux between Control simulation and NDAWN observations where reds indicate Control simulation SW was higher and blues indicate Control simulation SW was lower than NDAWN observations. (f) as in (e) but for Chemistry simulation.</p>	32
11	<p>RMSEs of surface downward shortwave flux (SW flux) from WRF-Chem throughout the 72-hr WRF-Chem simulations. The left-hand axis indicates RMSE with red dots being for the control simulation and blue for the chemistry simulation. A total of 75 NDAWN stations are used to calculate the values for each time step.</p>	33
12	<p>Box and whiskers time series plot for SW flux analysis minus observation differences. Red represents the WRF-Chem control simulation and blue represents the WRF-Chem chemistry simulation. Dots represent data outliers for that time.</p>	34
13	<p>As with Figure 10, but for 2m temperature. Observations included in (e) and (f) are from both ASOS and NDAWN station datasets.</p>	36
14	<p>Similar to Figure 11 but for 2m temperature. The right-hand axis and green bars indicate the number of observations used to calculate the RMSE for that time.</p>	37
15	<p>As in Figure 12 but for 2m temperature.</p>	38

16	Difference in 10m wind speed between (a) WRF-Chem control simulation and observations from ASOS stations and (b) as in (a) but for chemistry simulation. (c) Similar to Figure 11 and Figure 14 but for 10m wind speed.	39
17	As in Figure 12 and Figure 15 but for 10m wind speed.	40
18	(a) PBL heights for WRF-Chem control simulation on 29 June at 18Z, (b) as in (a) but for chemistry simulation, (c) difference plot of chemistry minus control simulations where red areas indicate the chemistry simulation has higher PBL heights and blue areas indicate the chemistry simulation has lower PBL heights compared to the control simulation, and (d) WRF-Chem AOD for reference.	42
19	(a) Aberdeen, SD PBL heights throughout the WRF-Chem 72-hr simulations. The control simulation is represented by the dashed orange line, the chemistry simulation represented by the solid blue line, and radiosonde derived PBL height observations are indicated by the black stars. (b) as in (a) but for Bismarck, ND	43
20	AOD as observed by AERONET (500 nm; black stars) an WRF-Chem simulations (550 nm) initialized with NAM Analysis data (solid line), and NAM forecast data (dotted lines).	45
21	(a) RMSE time series of SW flux for each of the five WRF-Chem Control simulations. Each run is denoted by a different symbol and color shade. (b) Same as (a), but for Chemistry simulations. (c) RMSE of SW flux 24 hours after initialization for all WRF-Chem simulations binned by AODs of 0.5.	47
22	As in Figure 21, but for 2m temperature.	49
23	As in Figure 21 and Figure 22, but for 10m wind speed.	51

LIST OF TABLES

Table		Page
1	WRF-Chem meteorological configurations.	13
2	WRF-Chem model parameterizations.	14

ACKNOWLEDGMENTS

I would like to thank my advisor, Dr. Jianglong Zhang, and my committee members, Dr. Aaron Kennedy and Dr. Frank Bowman, for the guidance and support throughout my studies and research. I would also like to thank Dr. Jeffrey Reid and Dr. Peng Xian from the Naval Research Laboratory for the NAAPS data and for their constructive comments/suggestions throughout this study.

A huge thank you to Jared Marquis for the patience, help, and advice (including teaching me WRF and providing editing feedback), and an even bigger thank you for the countless hours spent encouraging, motivating, and loving me when I struggled to do so on my own. I also appreciate you keeping our girls happy and healthy while I worked late nights on homework and thesis work.

Thank you to Melissa and Travis for keeping me grounded as only siblings can do and for sending memes and cat videos to distract me when I was banging my head against the computer.

I am forever thankful for the friendships forged over complaining about equations, how cold it is outside, and crafting. Grad school and North Dakota would have been a lot duller without you.

My gratitude must also be extended to the family and friends near and far that helped support me, checked in with me, let me vent my frustrations, and have seen me through the last few years.

Finally, I'd like to thank my sweet girls, Hailey, Macha, and Kona, for the unconditional love, cuddles, and puppy kisses no matter what obstacles we were facing.

This research was supported by the NSF grant OIA-1355466. The AERONET data were obtained from the NASA AERONET site (https://aeronet.gsfc.nasa.gov/new_web/aerosols.html). I acknowledge the use of imagery from the NASA Worldview application (<https://worldview.earthdata.nasa.gov>), part of the NASA Earth Observing System Data and Information System (EOSDIS).

This thesis is dedicated to Jared, Melissa, Travis, Hailey, Macha, and Kona who each remind me to keep chasing my dreams and give me unwavering support in their own weird ways. Thank you from the bottom of my heart.

ABSTRACT

When unaccounted for in numerical weather prediction (NWP) models, heavy aerosol events can cause significant unrealized biases in forecasted meteorological parameters such as surface temperature. A novel concept is proposed in this study to dynamically downscale aerosol fields from a global chemical transport model into a higher resolution NWP model to improve the near-surface forecasting accuracies during heavy aerosol events like biomass burning events. This concept is tested for a major biomass burning aerosol event over the Northern Great Plains region of the United States that occurred from 28 June – 4 July 2015. Aerosol analyses from the Navy Aerosol Analysis and Prediction System (NAAPS) are used as initial and boundary conditions for Weather Research and Forecasting with Chemistry (WRF-Chem) simulations. Through incorporating more realistic aerosol direct effects into the WRF-Chem simulations, errors in WRF-Chem simulated surface downward short-wave radiation, near-surface temperature, and near-surface wind speed are reduced compared with surface-based observations. This study confirms the ability to dynamically downscale analyses and forecasts from a global transport model to decrease aerosol direct effect induced biases for regional NWP forecasts during high-impact continental-scale aerosol events.

CHAPTER 1

INTRODUCTION

Aerosols are defined as solid or liquid particles suspended in the atmosphere. Atmospheric aerosols can be classified as *primary* or *secondary* aerosols based on their origins. Primary aerosols are aerosols emitted directly into the atmosphere from emission sources such as volcanic eruptions, sea spray, and combustion engines, whereas secondary aerosols form after reacting in the atmosphere (Clement and Ford, 1999; Pryor et al., 2015). Atmospheric aerosols can also be categorized into smoke (including black and organic carbons), dust, sea salt, and pollutant aerosols based on their physical and optical properties (e.g., Zhang et al., 2008).

Aerosols can directly affect climate and weather through the scattering and absorption of solar and terrestrial radiation. Numerous studies suggest that the presence of thick aerosol plumes attenuate surface-reaching solar energy, thereby causing significantly reduced surface temperature (e.g., Westphal et al., 1991; Robock et al., 1991; Kaufman and Koren, 2006; Jin et al., 2010; IPCC, 2014). Furthermore, aerosols can behave as cloud condensation nuclei (CCN) and indirectly affect climate by altering cloud droplet size distribution, changing cloud cover and lifespan, and potentially influencing precipitation. For example, Feingold et al. (2005) suggested that cooler temperatures due to the presence of a smoke plume may lead to a reduction in the cloud fraction. Yet, above a cloud, aerosols could increase the cloud amount due to the plume preventing moisture evaporation by the sun (Feingold et al., 2005).

Some recent studies have reported that aerosol events may influence the accuracy of regional weather forecasts. For instance, noticeable high biases were found in numerical weather prediction (NWP) model forecasted surface temperatures over Grand Forks, North Dakota when a smoke aerosol plume passed over the region during June-July 2015 (Zhang et al., 2016). Still, although evidenced from observational-based studies, the impacts of aerosols on operational NWP are largely unconsidered.

There are numerous complexities that lead to the exclusion of aerosols from operational NWP models. One of the major limitations that operational forecasting centers face is the computational expense associated with incorporating prognostic aerosols into NWP models (Benedetti et al., 2018). Additionally, aerosol impacts on weather forecasts are only significant for heavy aerosol events like biomass burning events or dust plumes. Even then, heavy aerosol episodes are regional and temporally sporadic (Zhang et al., 2016). Therefore, the benefit to operational forecasting centers of fully incorporating aerosols into NWP models remains unclear.

Still, some operational centers are currently working towards the incorporation of aerosol models into NWP models. For example, the new Global Atmosphere 7.0 and Global Land 7.0 (GA7.0/GL7.0) Unified Model from the Met Office incorporates the UK Chemistry and Aerosol GLOMAP-mode for aerosol processes (Walters et al., 2019). In another example, the High Resolution Rapid Refresh-Smoke (HRRR-Smoke) model is an experimental model being developed for operation based on WRF-Chem. HRRR-Smoke uses satellite-detected fires to forecast air quality, visibility, and aerosol-meteorological interactions in the continental United States four times daily (00, 06, 12, and 18 UTC) at a high spatial resolution (Ahmadov et al., 2019).

Theoretically, it is computationally expensive and unnecessary to fully incorporate aerosol effects into NWP models for regions and seasons with climatologically low aerosol loadings (e.g., Zhang et al., 2016). As an alternative, this study explores

the possibility of improving forecast accuracies of NWP models on an event-based, as-needed basis through dynamically downscaling aerosol fields from global chemical transport models (CTMs) to NWP models. One of the design purposes of this study is to use CTM data for improving NWP forecasts leading up to and during significant aerosol events only. During CTM-predicted low aerosol-loading days, CTM data are not downscaled into NWP models so as to save computational resources.

Global CTMs simulate aerosol emission, transport, and deposition with the use of meteorological fields from NWP models. In these CTMs, sources and sinks of various aerosol species are modeled, while the transport of aerosols is governed by meteorological fields from NWP models. It is important to understand that in models that have inline aerosol transport, feedback mechanisms are often not enabled between the aerosol and meteorological fields. Still, CTMs are computationally inexpensive and serve their purposes for operational aerosol, air quality, and visibility forecasts (e.g., Lynch et al., 2016; Y. Zhang, 2008; Baklanov et al., 2014).

In this study, the concept of improving NWP forecast accuracy by dynamically downscaling aerosol properties from a CTM to an NWP model during an aerosol episode is explored over the Northern Great Plains in 2015. CTM aerosol fields from a CTM-predicted significant aerosol event are dynamically downscaled and incorporated into an NWP model to account for direct radiative impacts of aerosols on meteorological features. The CTM used in this study is the Navy Aerosol Analysis and Prediction System (NAAPS; Lynch et al., 2016), which is driven by meteorological fields from the Navy Global Environmental Model (NAVGEM; Hogan et al., 2014). The NWP model used in this study is the Weather Research and Forecasting Model with Chemistry (WRF-Chem), which has the capability of accounting for the direct and indirect aerosol impacts on weather (Skamarock et al., 2008; Grell et al., 2005; Fast et al., 2006; Peckham et al., 2011; and Powers et al., 2016), although

aerosol direct impacts are the focus of this study. Due to the study domain being largely limited to surface observations for the study period, the emphasis is given to evaluate modeled near-surface properties such as temperature, downwelling shortwave radiation, and wind speed.

This thesis is organized as follows: Chapter 2 discusses the aerosol event used as a case study for a novel event-drive forecasting approach, Chapter 3 discusses the models and datasets for this study, Chapter 4 discusses the methods behind this study, Chapter 5 explains the results, and Chapter 6 summarizes major conclusions of this study.

CHAPTER 2

BACKGROUND

To evaluate the feasibility of dynamically downscaling global CTM data for regional weather forecasts, an extreme smoke event is selected that occurred in the Northern Great Plains (NGP) region. Around 23 June 2015, numerous wildfires were initiated in the Northwest Territories, northern Alberta, and Saskatchewan in Canada. Assumedly caused by lightning from recent widespread thunderstorms throughout central Canada, a minimum of 60 individual fires or complexes were visible in the MODIS fire product (Zhang et al., 2016). At least 30 separate fires had burned more than 1,000 hectares each by 27 June when massive smoke plumes were visible on MODIS imagery over central Canada (Zhang et al., 2016). Another surge of wildfire smoke occurred on 28 June when existing wildfires escalated, and additional wildfires formed in western Manitoba (Figure 1a). At this point, a substantial smoke plume was already present throughout central Canada and began advecting over the Dakotas and Nebraska in the US.

Leading up to the June 2015 smoke event, western Canada had experienced a drier and warmer summer than average. While the Canadian wildfires were increasing in number and size, a persistent longwave trough built over western Canada and the western US on 27 June 2015. By 28 June, MODIS imagery showed the massive smoke plume intensifying in central Canada and its initial entrance into the US. Figure 2 shows strong west-northwesterly winds at 700 hPa occurred in the NGP region over three days during the smoke event. These winds veered to north-northwesterly at

500 hPa ultimately causing a massive river of smoke to advect into the Dakotas and Nebraska.

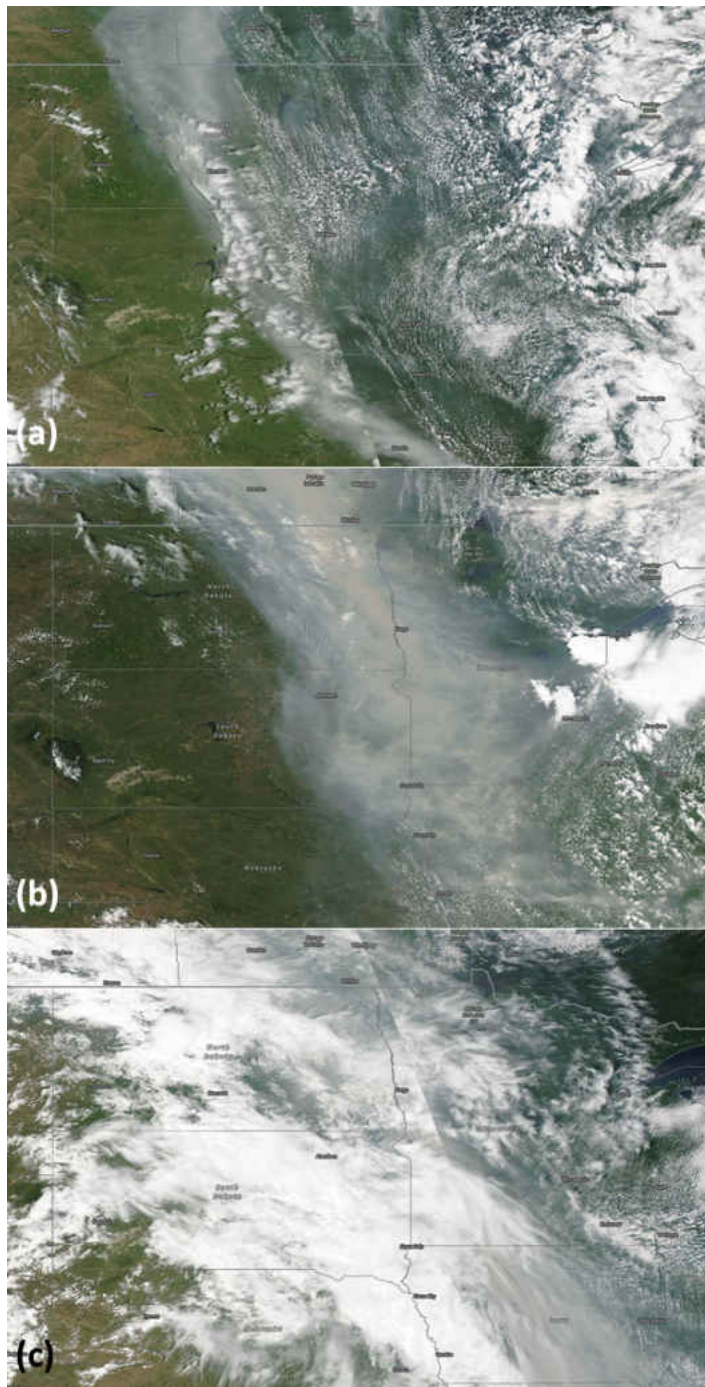


Figure 1: NASA Worldview Aqua MODIS visible imagery for (a) 20:25 UTC on 28 June, (b) 19:30 UTC on 29 June, and (c) 20:15 UTC on 30 June 2015. From NASA Worldview

The most dramatic day of the smoke event for the region occurred on 29 June 2015. A fast-moving shortwave trough enhanced the already rapidly transported smoke plume from central Canada into the Midwest and Upper Mississippi and Ohio River Valleys (Figure 1b). West-northwesterly winds increased from 10 m/s at 950 hPa to 25 m/s at 500 hPa (22 mph to 55 mph, respectively) at 18Z, which appears to be the peak of the smoke event due to the high optical depth.

By 30 June, smoke extended to the Carolinas and Georgia, but became much more diffuse over the Midwest and the Upper Mississippi and Ohio River Valleys (Figure 1c). Heavy cloud cover and rain – courtesy of a weak midlatitude cyclone – helped to clear out the smoke. A low-pressure system and an occluded front moved into the Dakotas producing heavy cloud cover, rain, and more zonal winds. As a result, transport of smoke into the region lessened, and the smoke in the region was able to diminish. Independently, wildfire activity related to this smoke event began to diminish as well, further curtailing the smoke plume. A significant cold front in western and central Canada on 6 July helped extinguish the wildfires, effectively ending the smoke event.

Only two valid radiosonde releases occurred throughout this smoke event within proximity to the smoke plume. The Bismarck, ND and International Falls, MN NWS office balloon launches were unable to collect useful data from the plume due to the plume’s trajectory on 29-30 June, and similarly for the Omaha/Topeka/Spring corridor to the south. However, the Aberdeen, South Dakota office’s 29 June launch at 12Z and 30 June launch at 00Z were successful in penetrating the edge of the smoke plume. Due to solar flare activity, CALIPSO observations – which can be used to derive vertical distributions of plumes – were also unavailable to analyze the smoke plume until 30 June. Zhang et al. (2016) suggested the plume was most likely in the

lower to middle troposphere – specifically less than 5 km in altitude – based on the Aberdeen soundings and lack of significant increase in surface smoke observation.

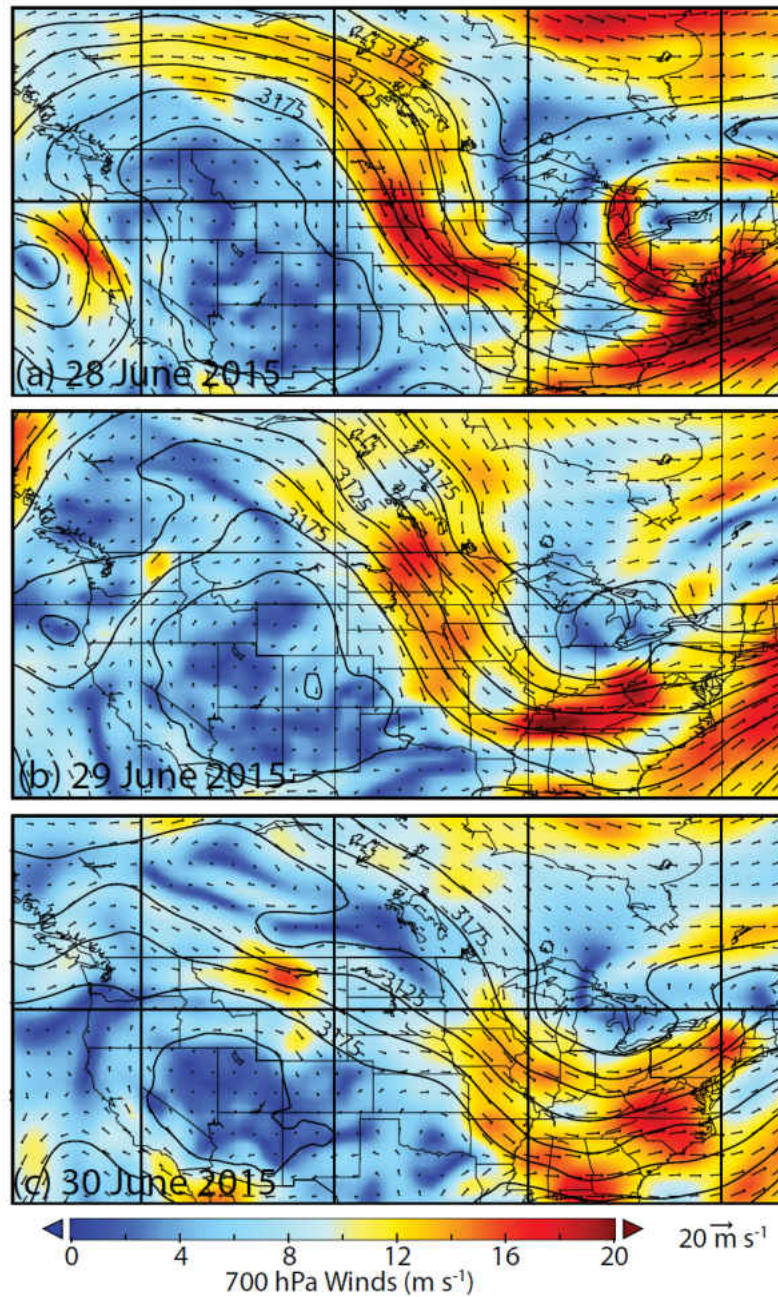


Figure 2: ECMWF Reanalysis of 700 hPa geopotential heights overlaid on winds for (a) 28 June, (b) 29 June, and (c) 30 June 2015 at 18Z. From Zhang et al., 2016

The aforementioned late-June 2015 smoke event was examined by Zhang et al. (2016) at length. The Zhang et al. (2016) study found that the Grand Forks, ND NWS office overestimated the maximum surface temperature on 29 June by 2-5°C (Figure 3). By comparison, Bismarck, an area not directly impacted by the smoke event, underestimated the surface temperature on 29 June by 1°C. The significant overestimation by the Grand Forks NWS is likely a direct consequence of operational models not accounting for aerosol events within the model and, therefore, forecasters are left unaware of the significant aerosol impacts to come.

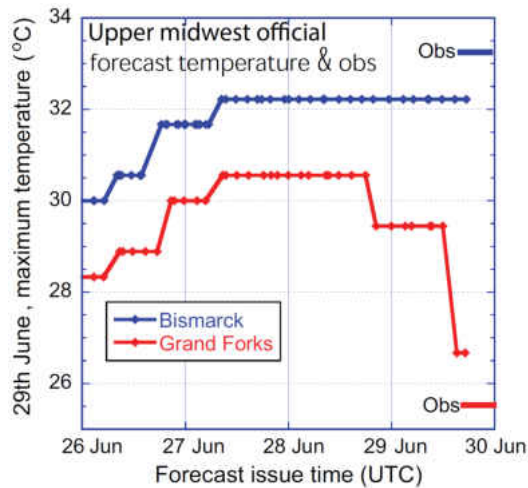


Figure 3: A time series of forecasted maximum temperature for 29 June 2015 at Bismarck (blue) and Grand Forks (red) National Weather Service offices. Observed maximum temperatures for 29 June are indicated by the short lines on right-hand side of plot at each NWS office. From Zhang et al., 2016.

In addition, a direct surface cooling efficiency was calculated for aerosol optical depth (AOD) at a wavelength of 550 nm (AOD_{550}). AOD is a unitless measure of how much sunlight is absorbed or scattered (i.e., “blocked”) by particles in the atmosphere before reaching the Earth’s surface. For this event, the presence of aerosols caused the surface temperature to decrease by approximately 1.5°C per unit AOD_{550} than if the aerosols were not present. For example, the AErosol RObotic NETwork (AERONET)

in Grand Forks, North Dakota reported a peak AOD of nearly 5.0 on 29 June 2015. Based on the relationship in Zhang et al. (2016), Grand Forks should have experienced surface cooling of approximately 7.5°C due to the smoke plume. This is largely consistent with the Grand Forks' $\sim 5.0^{\circ}\text{C}$ surface temperature forecast error (Figure 3).

Finally, Zhang et al. (2016) pointed out several areas of concern when studying regional extreme aerosol events. For one, aerosol plumes with extreme high aerosol loadings can be (and likely were in the June 2015 smoke event) misidentified by MODIS DT/DB retrievals as cloud (Alfaro-Contreras et al., 2016). Moreover, daily AOD_{550} changes greater than 1.0 are relatively rare events on a global scale. Based on the direct surface cooling efficiency, inclusion of aerosol events of this magnitude are unlikely to significantly improve the global accuracy of near-surface air temperature forecasts. This is exacerbated by the fact that temperature changes due to low-to-moderate aerosol plumes are typically within the bounds of model uncertainties. However, as discussed previously, some regions are more prone to significant aerosol events, suggesting that inclusion of aerosols in NWP forecasts for event- or regional-based forecasts may be beneficial where significant daily changes in AOD exist.

CHAPTER 3

MODELS AND DATASETS

The smoke event described in Chapter 2 is simulated using the Weather Research and Forecasting with Chemistry (WRF-Chem) model in this study. The Navy Aerosol Analysis and Prediction System (NAAPS) chemical transport model data are dynamically downscaled into WRF-Chem and provide aerosol fields for WRF-Chem simulation. To assist the model analyses, North American Mesoscale (NAM) analysis and forecast data are used to initialize WRF-Chem simulations. Observation datasets are also used for evaluating and verifying the coupled WRF-Chem and NAAPS model simulations.

3.1 WRF-Chem

The WRF model is a mesoscale NWP model made for the purposes of providing operational weather forecasts and conducting atmospheric research (Skamarock et al., 2008). This study utilizes the Advanced Research WRF (ARW) modeling system Version 3.9. The simulation period of interest begins 28 June 2015 at 00 UTC prior to the major smoke plume entering the study domain, and spans through 01 July 2015 at 00 UTC after the peak of the smoke event occurred in eastern North Dakota. This allows approximately 12 hours of model spin-up prior to the significant smoke aerosol event advecting into the region on 28 June 2015. The model domain contains 100 by 100 horizontal grid points at 12 km grid spacing that centers in southeast North Dakota (40.32°N - 51.11°N , 89.21°W - 105.92°W ; Figure 4). In the vertical,

terrain-following sigma coordinates are utilized with 40 layers. This system allows for finer vertical spacing near the surface with deeper layer aloft as pressure exponentially decreases in the upper atmosphere. A summary of model configurations can be found in Table 1.

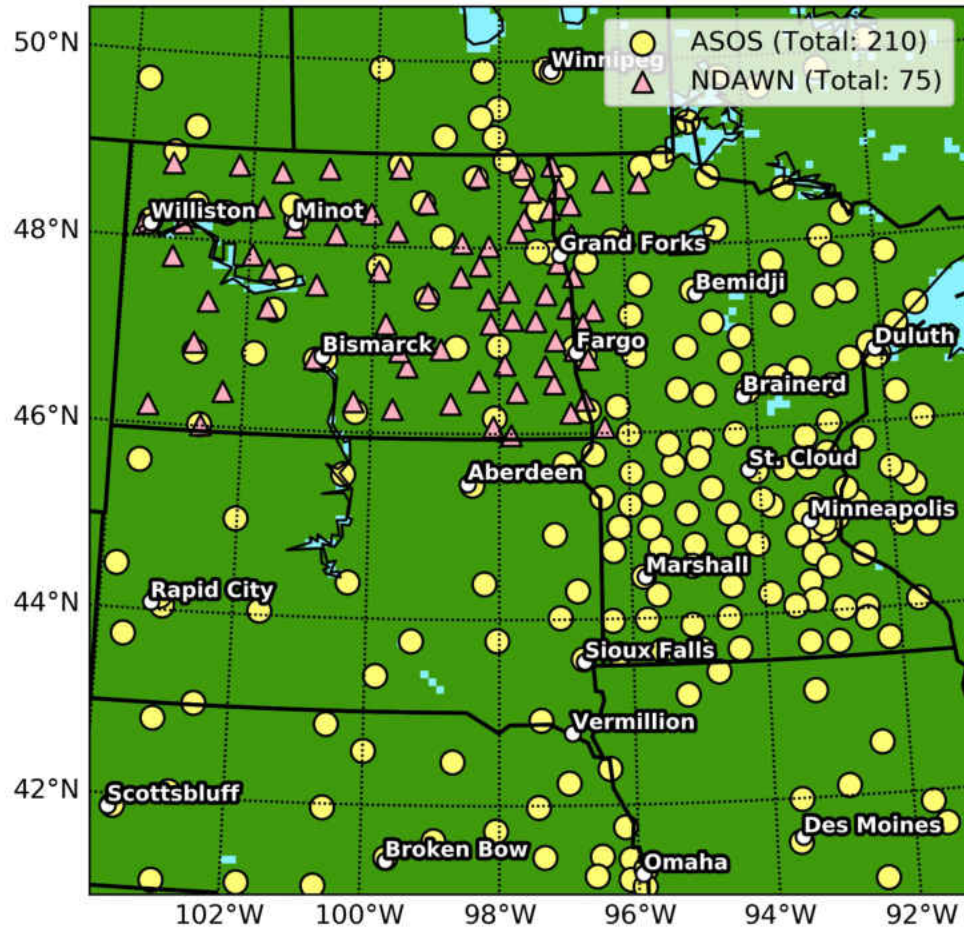


Figure 4: Depiction of the WRF-Chem model domain used in this study. Yellow circles represent ASOS stations and pink triangles represent NDAWN stations used in this study

In addition to the meteorological simulations provided by ARW, atmospheric chemistry is included in these simulations using the WRF-Chem package. The ARW system built with the WRF-Chem package are henceforth referred to as WRF-Chem in this study. WRF-Chem is capable of being operated in a variety of spatial and

Table 1: WRF-Chem meteorological configurations.

Label	Description
Model	WRF-Chem Version 3.9
Simulation Period	28 June - 01 July 2015
Horizontal Resolution	12 km
Dimensions (x,y)	100, 100
Vertical Levels	40
Meteorological Boundary Conditions	NCEP NAM 12 km Analysis
Chemistry Boundary Conditions	NAAPS
Boundary Conditions Interval	10800 sec (3hr)
Time Step	60 sec
Model Top	5000 Pa (50 hPa)
Damping Layer	5000 m

temporal resolutions as an offline model and up to a significantly-coupled online model.

Parameterization schemes and model configurations used in the study – including microphysics, radiation, planetary boundary layer, cumulus, land surface model, aerosol, and dry deposition schemes – are summarized in Table 2. This study utilizes the Georgia Institute of Technology-Goddard global Ozone Chemistry Aerosol Radiation and Transport (GOCART) aerosol scheme (Ginoux et al., 2001). Longwave and shortwave radiation parameterizations both use the Rapid Radiative Transfer Model for GCMs (RRTMG) scheme that is able to simulate direct aerosol effects through direct coupling with the GOCART aerosol module (WRF-Chem V. 3.9.1.1 User’s Guide). The indirect effect is not investigated within this study. As such, the Kain-Fritsch simple cloud model cumulus scheme is used as the cumulus parameterization.

Table 2: WRF-Chem model parameterizations.

Option	Scheme	Reference
Microphysics	Lin et al.	Chen and Sun (2002)
Longwave Radiation	RRTMG	Iacono et al. (2008)
Shortwave Radiation	RRTMG	Iacono et al. (2008)
Planetary Boundary Layer	Yonsei University (YSU)	Hong et al. (2006)
Cumulus	Kain-Fritsch	Kain (2004)
Land Surface model	Noah	Chen and Dudhia (2001)
Aerosol Mechanism	GOCART simple aerosol	Ginoux et al. (2001)
Aerosol Model	GOCART	Ginoux et al. (2001)
Dry Deposition	Included	N/A

3.2 Navy Aerosol Analysis and Prediction System (NAAPS)

The Navy Aerosol Analysis and Prediction System (NAAPS) model is an operational aerosol transport model that produces forecasts of three-dimensional aerosol concentrations on a global scale for four aerosol species including anthropogenic and biogenic fine aerosols, smoke, sea salt, and dust (Lynch et al., 2016). In operational runs, global aerosol concentrations are simulated every six hours. In research mode, global aerosol fields can also be generated at a shorter temporal resolution (e.g., every three hours). Meteorology is provided to NAAPS by the Navy Global Environmental Model (NAVGEM), which is an operational global weather prediction system produced by the United States Navy (Hogan, 2014). Research-mode NAAPS simulations used in this study have $1^\circ \times 1^\circ$ (Latitude/Longitude) horizontal resolution with 25 vertical pressure levels (Lynch et al., 2016). Finally, NAAPS analyses and forecasts are assisted with the assimilation of Terra and Aqua MODerate resolution Imaging Spectroradiometer (MODIS) optical depth data (e.g., Levy et al., 2013). For these research runs, Terra Multi-angle Imaging Spectroradiometer (MISR) aerosol products are assimilated as well (Kahn et al., 2010; Shi et al., 2014). Note that both

Terra and Aqua are sun-synchronous, near-polar orbiting satellites, and thus, each sensor provides approximately one overpass per day over the study region (Zhang et al., 2008).

In this study, smoke mass concentration data from the research version of NAAPS is interpolated to the WRF-Chem grid to be utilized as WRF-Chem’s aerosol initial conditions and boundary conditions. To better represent the smoke event, NAAPS simulations are adjusted based on observed aerosol properties. In particular, the smoke injection height at the point of emission has been set to between two and three kilometers based on lidar observations from the Cloud-Aerosol Transport System (CATS) onboard the International Space Station (Yorks et al., 2014). Next, the emission source smoke flux is arbitrarily doubled to nudge the NAAPS simulated smoke plumes towards the ground-based AOD observations at the Grand Forks, ND AERONET site (47.912°N, 97.325°W). Finally, the AOD data assimilation frequency is increased from every six hours to every three hours. Still, as mentioned above, one daytime overpass per day per sensor is expected for the Terra and Aqua MODIS as well as Terra MISR AOD values used in the assimilation process over the study region (Zhang et al., 2008; Lynch et al., 2016).

NAAPS simulated smoke aerosols are represented by four biomass burning related aerosol species in the GOCART aerosol scheme implemented in WRF-Chem: hydrophobic black carbon, hydrophilic black carbon, hydrophobic organic carbon, and hydrophilic organic carbon. Therefore, NAAPS smoke aerosol data must be converted into the four smoke aerosol categories for ingest into WRF-Chem. Hydrophobic (hydrophilic) black carbon is comprised of fresh (aged/coated) soot, while hydrophobic (hydrophilic) organic carbon is comprised of fresh burnt (aged/coated) biomass. To convert NAAPS smoke aerosols to the four types of biomass burning aerosols (as defined by WRF-Chem’s GOCART aerosol scheme), the ratio of black

carbon to organic carbon in a smoke plume is assumed to be 1:7 (Liousse et al., 1996). Black carbon is assumed to be 80% comprised of hydrophilic black carbon particles, with the remaining 20% being hydrophobic (Cooke et al., 1999). Similarly, 50% of organic carbon is hydrophilic, while 50% is assumed to be hydrophobic (Cooke et al., 1999).

NAAPS reports aerosol concentrations in units of $\mu g/m^3$, whereas WRF-Chem aerosol fields are quantified in $\mu g/kg - dryair$. Thus, aerosol mass concentrations from NAAPS are converted to aerosol mixing ratio as needed for ingest into WRF-Chem. Aerosol concentration is calculated from mixing ratio using density as follows:

$$C_{NAAPS} = w_{aerosol} \times \rho_{NAAPS} \quad (3.1)$$

where c_{NAAPS} is the NAAPS aerosol mass concentration in units of $\mu g/m^3$, $w_{aerosol}$ is the mixing ratio in units of $\mu g/kg - dryair$, and ρ_{NAAPS} is the ambient air density at that grid point. However, density is not directly measurable in the atmosphere. Thus, density can be substituted by the ideal gas law. With this substitution and by solving for $w_{aerosol}$, the WRF-Chem aerosol mixing ratio can be calculated with the following equation at each vertical level for each NAAPS grid point:

$$w_{aerosol} = \frac{c_{NAAPS} \times R_d \times T_{NAAPS}}{p_{NAAPS}} \quad (3.2)$$

where R_d is the dry air gas constant and T_{NAAPS} and p_{NAAPS} are the ambient temperature and pressure, respectively, for a given location at a given NAAPS layer.

3.3 North American Mesoscale (NAM) Analyses and Forecasts

To construct WRF-Chem analyses, the 12 km North American Mesoscale (NAM) model analyses are used as initial and boundary conditions (<https://www.ncdc.gov>).

noaa.gov/data-access/model-datasets/north-american-mesoscale-forecast-system-nam; last accessed on April 22, 2020). Initial conditions are inputs for the model that describe the meteorological conditions throughout the entire domain when the model is initialized. Boundary conditions are ingested at pre-determined regular intervals throughout the simulation at the boundaries of the WRF-Chem domain.

NAM analyses cover the continental United States with a 12 km spatial resolution, and are available every six hours (00, 06, 12, and 18 UTC) for 40 pressure levels. To further examine the impacts on WRF-Chem forecast parameters, the NAM 12 km forecast data archived by the National Centers for Environmental Information (NCEI) are also used in this study. Different from the NAM analyses, which are constructed through ingesting gridded observational data, observations are not used beyond initialization in NAM 12 km archived forecasts. Thus, NAM forecasts are considered to be less accurate than NAM analyses. In addition to WRF-Chem analyses using the NAM analysis data, a forecast sensitivity study is conducted (see Chapter 4) with 48-hour forecasts initialized every six hours from 00 UTC 28 June 2015 to 00 UTC 29 June 2015 using the archived forecast meteorological fields from NAM as initial and boundary conditions.

3.4 Automated Surface Observing System (ASOS) and North Dakota Agricultural Weather Network (NDAWN) Data

Surface meteorological observations are used to evaluate WRF-Chem simulations. Automated Surface Observing System (ASOS) station data provides surface or near-surface measurements of meteorological parameters including 2-meter (2m) air temperature and 10-meter (10m) wind speed for model evaluation. The ASOS data are obtained from the Iowa State University Environmental Mesonet (<https://mesonet>).

agron.iastate.edu/; last accessed April 22, 2020). A total of 210 ASOS stations within the study domain are used in this study.

To complement the ASOS data, North Dakota Agricultural Weather Network (NDAWN) observations (<https://ndawn.ndus.nodak.edu/>; last accessed on July 22, 2020) are also used for evaluating WRF-Chem modeled surface downward shortwave radiation fluxes and near-surface temperature. NDAWN data are available at weather stations throughout North Dakota and select sites in Montana and Minnesota towns near North Dakota borders. While this does not encompass the entire focus area for this study, it does provide a set of surface downward shortwave radiation observations for a small area of the domain, and is included in this study for verification purposes. Wind speed and direction data are also available from the NDAWN data, but are recorded at three meters. Thus, NDAWN wind data are not used. A total of 75 NDAWN stations within the study domain are used in this study. Figure 4 shows the spatial distribution of ASOS stations and NDAWN sites.

3.5 Aerosol Robotic Network (AERONET) Data

NAAPS and WRF-Chem simulated AOD values are also inter-compared with Aerosol Robotic Network (AERONET) observations recorded at the Grand Forks, ND AERONET site (47.912°N, 97.325°W). AOD values from AERONET sites are derived by measuring the attenuated solar energy at seven wavelengths ranging from 340 nm to 1020 nm using Beer’s Law (Holben et al., 1998). The cloud cleared and quality assured level 2 version 3 AERONET data are used. The accuracy of AERONET AODs are on the order of 0.01 – 0.02 (Eck et al., 1999).



Figure 5: Image of the AERONET site located in Grand Forks, ND. Photo from Grand Forks, ND AERONET website by NASA (https://aeronet.gsfc.nasa.gov/new_web/photo_db_v3/Grand_Forks.html).

CHAPTER 4

METHODS

4.1 Experimental Design

The impacts of aerosol plumes on WRF-Chem forecasts using NAM analyses and NAM forecasts are studied by examining the differences in WRF-Chem simulations with (chemistry simulation or run) and without (control simulation or run) including aerosol fields from NAAPS as illustrated in Figure 6.

For the control simulations, WRF-Chem simulations are conducted without inclusion of chemistry or aerosol data. Geological and meteorological data are pre-processed and reformatted using the WRF Pre-processing System (WPS) for the WRF-Chem runs – including trimming the input datasets to the domain focus area. Geographical data are modified to the domain grids and meteorological fields are horizontally interpolated to the user-defined domain. User-defined vertical levels for meteorological variables and initial and boundary conditions are also derived based on the pre-processed meteorological files.

For the WRF-Chem aerosol runs (or dynamically downscaled runs), additional steps are taken for inclusion of NAAPS aerosol fields as initial conditions and boundary conditions for aerosols (see steps outlined by black box in Figure 6). In this study, aerosol boundary conditions from NAAPS are ingested every three hours. More detailed steps for modifying WRF-Chem initial and boundary conditions using NAAPS data are described below.

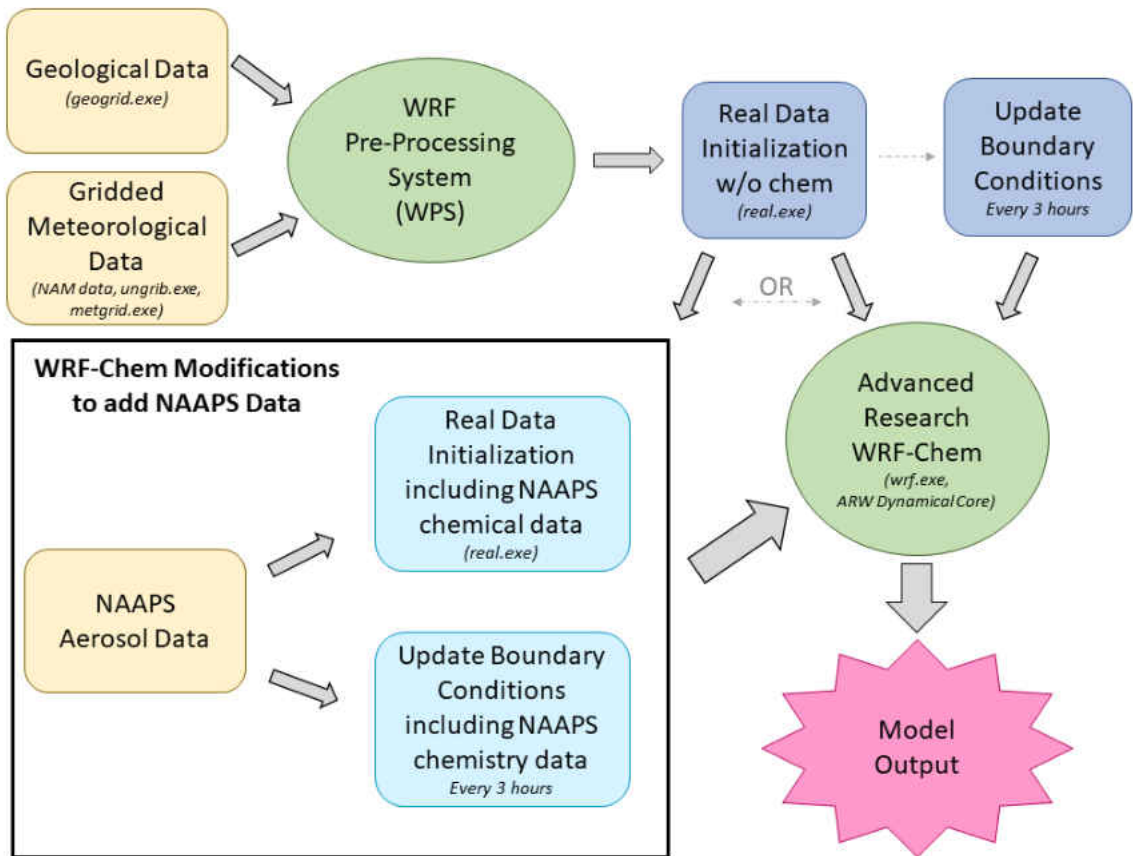


Figure 6: Flow chart representing the basic steps for running WRF-Chem with and without NAAPS data. The black outlined box includes extra steps necessary for including NAAPS aerosol data in WRF-Chem modeling.

4.1.1 Modification of WRF-Chem Initial Conditions for Aerosols

The WRF-Chem initial conditions file holds information for the model regarding the meteorological, chemical, and aerosol conditions at the time of model initialization throughout the entire domain at all vertical levels. Since the smoke plume originates outside the study area, the model domain here intentionally does not include emission sources for the smoke plume. As such, the initial condition file is modified to include NAAPS aerosol data for each WRF-Chem simulation.

NAAPS aerosol mass fields are vertically and horizontally interpolated to the WRF-Chem grid including the use of Equation 3.2 to generate aerosol mixing ratios.

In addition, the WRF-Chem above sea level (ASL) heights are also calculated based on Equation 4.1 to allow for interpolation between WRF-Chem and NAAPS vertical levels.

$$z = \frac{ph[level] + ph[level + 1]}{2g} \quad (4.1)$$

Here, z is the non-staggered WRF-Chem ASL height in meters, ph is the WRF-Chem geopotential height at a vertical level in units of m^2/s^2 , $[level]$ refers to the variable at a certain level, $[level + 1]$ is the variable at next vertical level, and g is the gravity in units of m/s^2 .

A trilinear interpolation is further implemented to interpolate NAAPS data to the WRF-Chem model grid ensuring that each WRF-Chem grid point has an associated NAAPS smoke aerosol value at each horizontal location and each vertical level. Values are calculated for each of the hydrophobic black carbon, hydrophilic black carbon, hydrophobic organic carbon, and hydrophilic organic carbon WRF-Chem variables based on the methods described in Section 3.2.

4.1.2 Modification of WRF-Chem Boundary Conditions for Aerosols

Boundary conditions allow for smooth transition of variables along the edges of the model domain as well as advection into and out of the domain. Because smoke is not originating from within the model domain, smoke plumes must be transported into the domain from the lateral boundaries throughout the simulation. As such, the lateral boundary conditions file is modified to include the NAAPS aerosol data. Besides the necessary modifications as mentioned in Section 4.1.1 (i.e., conversion of aerosol mass concentrations to mixing ratio), aerosol mixing ratio tendencies are needed at each boundary grid point to provide the model with aerosol information

at times where input aerosol data is unavailable. Tendency is simply the change in a variable from one boundary condition time step to the next. This is necessary because NAAPS aerosol fields are only ingested into the WRF-Chem simulation in 3-hr intervals whereas the model requires information at the boundaries for each model time step (i.e., 60 seconds for this study).

The aerosol mixing ratio tendency is calculated using the following relationship:

$$\text{Aerosol Mixing Ratio Tendency} = \frac{\omega[x, y, z, t + \Delta t] - \omega[x, y, z, t]}{\Delta t} \quad (4.2)$$

where $\omega[x, y, z, t + \Delta t]$ is the aerosol mixing ratio value at a given location (x, y, z) at times $(t + \Delta t)$ and t , respectively, and Δt is the boundary condition update interval. Aerosol mixing ratio tendencies are, thus, calculated at each model grid point along the boundaries with each boundary having a width of five grid points. That is, the width of the boundary extends five grid point rows/columns from the domain edge into the domain space (Figure 7). This boundary contains a “specified zone” where variables are not modified by the model (i.e., aerosol mixing ratio is always equal to the NAAPS analysis). For this study, the specified zone is one grid point wide. Grid points between the specified zone and the model domain are referred to as the “relaxation zone”. Relaxation rows/columns nudge the boundary conditions towards the model values preventing unrealistic errors from propagating through the model forecast due to issues such as discontinuities between the pre-described boundary conditions (e.g., aerosol from the NAAPS) and the calculated conditions within the model domain.

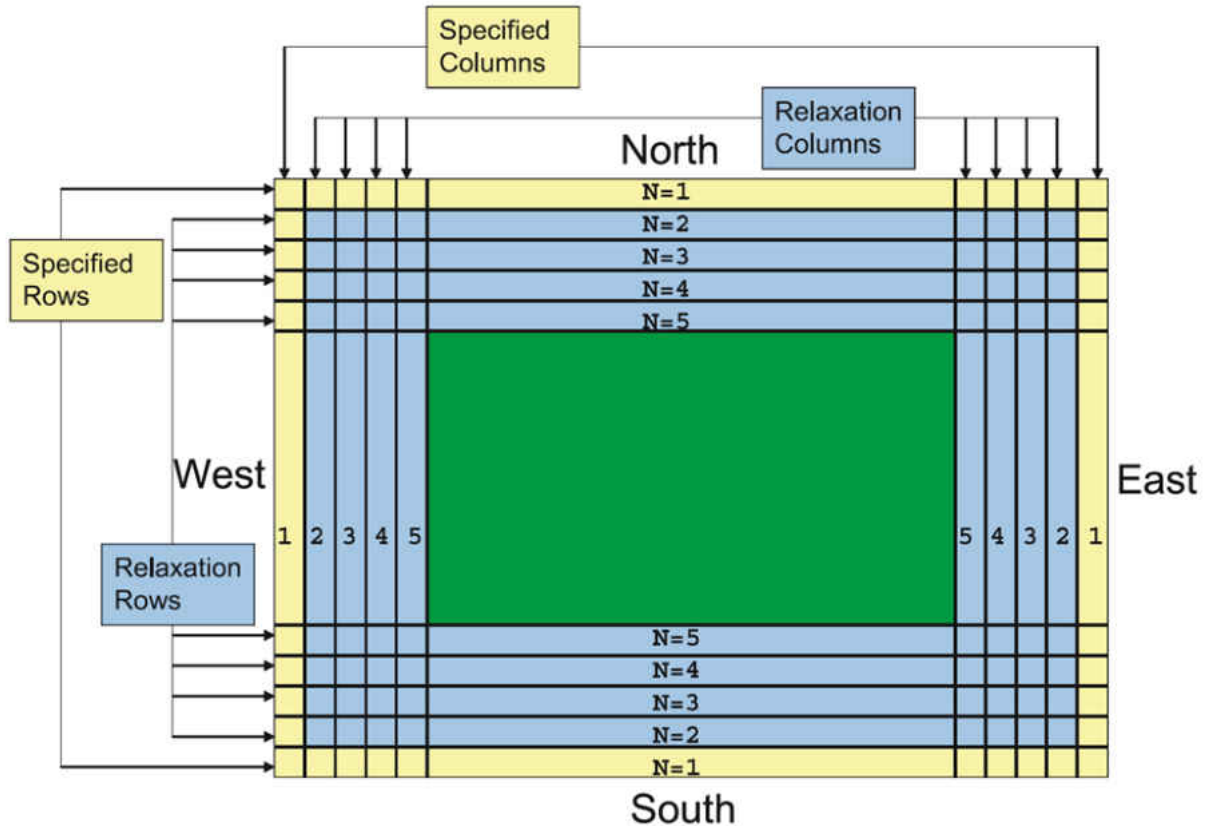


Figure 7: The four boundaries can be seen in this figure. The inner domain is colored in green. The boundary width is comprised of both the yellow specified rows/columns and blue relaxation rows/columns. Figure is from Skamarock et al. (2008).

Finally, the boundary conditions file does not include all diagnostic variables that can otherwise be found in the WRF-Chem output. Calculations for the boundary conditions are made by using several static variables found in the WRF-Chem namelist and initial conditions file: base-state geopotential height, base-state dry air mass in column, latitude, and longitude. In addition, the boundary condition file only contains the dry air mass in the column perturbation variable, “mu”, for each of the boundaries; thus, the mu base-state variable is also obtained from the initial

conditions file. Geopotential height is calculated for the lateral boundary conditions western edge as follows:

$$z_{(\text{west, staggered})} = \left(\frac{ph_{(\text{west})}}{\mu_{(\text{west, b})}} + ph_{(\text{west, b})} \right) \times \frac{1}{g} \quad (4.3)$$

where $z_{(\text{west, staggered})}$ is the staggered geopotential height for the western boundary, $ph_{(\text{west})}$ is the western boundary perturbation geopotential height from boundary conditions file, $\mu_{(\text{west, b})}$ is the base-state dry air mass in column from the initial conditions file, $ph_{(\text{west, b})}$ is the base-state geopotential height for the western boundary from the initial conditions file, and g is gravity (Skamarock et al., 2008). With that, the non-staggered value can be calculated for each vertical level by averaging the layer with the next. This process is repeated for each of the four boundaries. Thus, the above relationships are used to determine the NAAPS mixing ratios for the four types of carbon particles used in this study and their appropriate tendencies for inclusion in the boundary conditions file.

4.2 Aerosol Optical Depth Calculation

To evaluate the model performance against AERONET data, aerosol fields from WRF-Chem are converted to AOD values. These AOD values are computed based on the integration of aerosol extinction through the column as shown in Equation 4.4.

$$\tau_{550} = \sum (\beta_{550} \times dz) \quad (4.4)$$

Here, τ_{550} is the total column AOD at 550 nm (unitless), β_{550} is the extinction coefficient at 550 nm in units of m^{-1} from WRF-Chem output, and dz is the layer depth between vertical levels in units of m. Unless specifically mentioned, AOD refers to

AOD at 550 nm hereafter. The layer height is computed based upon the hydrostatic equation:

$$dz = \frac{p[l] - p[l - 1]}{\left(\frac{\rho[l] + \rho[l+1]}{2}\right) \times g} \quad (4.5)$$

where dz is the layer depth in m, p is the ambient pressure, ρ is the ambient density calculated via the ideal gas law, g is gravity, $[l]$ indicates the vertical level, and $[l - 1]$ indicates the next lower vertical level.

4.3 Evaluation Methods

WRF-Chem model simulation outputs are compared to NAAPS, ASOS, NDAWN, and AERONET data to analyze the performance of WRF-Chem simulations with and without inclusion of the NAAPS aerosol fields. To compare WRF-Chem aerosol fields with NAAPS data, both WRF-Chem and NAAPS outputs are co-located spatially and temporally. Only WRF-Chem and NAAPS data for the same time are used in the comparison. Spatially, a bilinear interpolation is conducted for WRF-Chem data after locating NAAPS output to the nearest WRF-Chem grid point.

Following similar methods, WRF-Chem is also co-located to ASOS and/or NDAWN data spatially and temporally for inter-comparing modeled meteorological fields for WRF-Chem and observed values from ASOS data. Observations are included in the comparisons based on several criteria. First, only ASOS and/or NDAWN data within one hour of the model output time are included. Next, ambient air temperature observations are assumed to be at two meters in height. Finally, ASOS observed wind variables (assumed to be at a height of 10m) are included in analysis. Wind speeds less than 2.5 knots are considered light and variable, and these observations are set to zero.

Finally, Root Mean Square Error (RMSE), as shown in Equation 4.6, is used for quantifying the uncertainties in the WRF-Chem modeled parameters.

$$\text{RMSE} = \sqrt{\frac{\sum_{i=1}^N (x_a - x_o)^2}{N}} \quad (4.6)$$

where x_a is the modeled parameter at the observation location, x_o is the observed parameter based on ASOS and/or NDAWN data, and N is the total number of observations.

CHAPTER 5

RESULTS AND DISCUSSIONS

In this section, the performance of WRF-Chem with dynamically downscaled NAAPS data is investigated through inter-comparison with NAAPS data, satellite images, and ground-based measurements for WRF-Chem simulations that use NAM analyses data (Sections 5.1-5.5). The impact of including aerosol fields from NAAPS is also quantified by comparing the WRF-Chem forecasted meteorological variables from the chemistry runs with WRF-Chem forecasts from the control runs (Section 5.6) in which only background aerosols are included (i.e., a control simulation meant to simulate the majority of current operational weather prediction systems).

5.1 Aerosol Optical Depth Analysis

To determine the accuracy of the WRF-Chem simulated aerosol fields initialized with NAAPS aerosol data, total column AODs from the WRF-Chem chemistry simulation are compared to the NAAPS-reported total column AODs for the study domain as shown in Figure 8. At the beginning of the study period (00Z, 28 July 2015), a maximum AOD of ~ 1.0 is found in NAAPS data just north of Winnipeg, MB in Canada (Figure 8a). This aerosol feature is not represented in the WRF-Chem simulation for the same time, as shown in Figure 8d. This is expected since NAAPS data had not yet advected into the WRF-Chem domain at initialization.

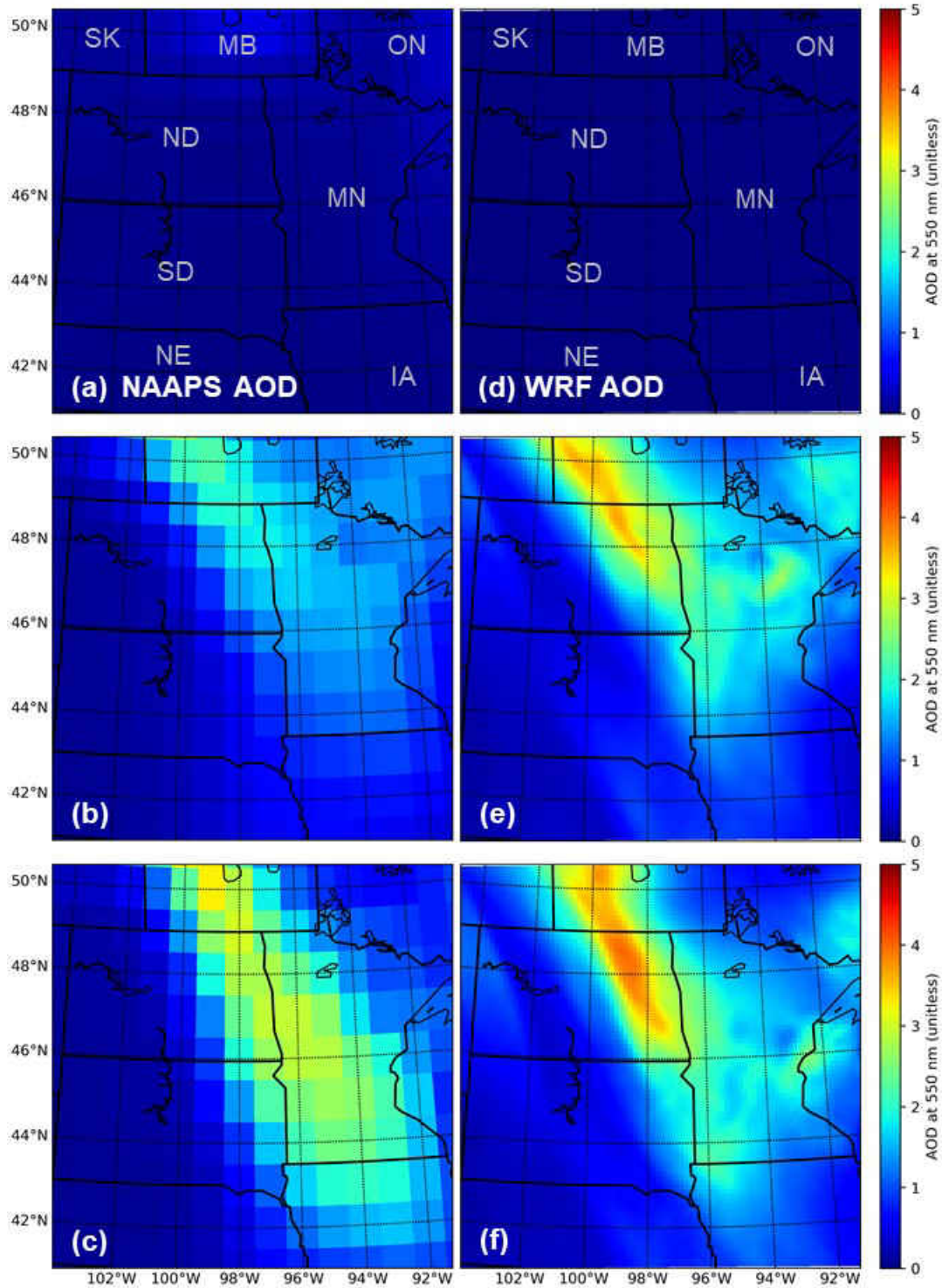


Figure 8: (a), (b), (c) Spatial distributions of NAAPS total column AOD spatial plots for the WRF-Chem domain for 28 Jun 2015 at 00Z, 29 Jun at 15Z, and 29 Jun at 18Z, respectively. (d), (e), (f) as in (a), (b), (c) but for WRF-Chem simulated total column AOD from the chemistry run.

At 15 UTC on 29 June 2015, a reasonable consensus is achieved between the NAAPS (Figure 8b) and WRF-Chem (Figure 8e) model simulations of total column AOD as the smoke event nears its optical peak in the NGP. Both NAAPS and WRF-Chem indicate the plume extends from eastern Saskatchewan and western Manitoba into eastern North Dakota and western Minnesota.

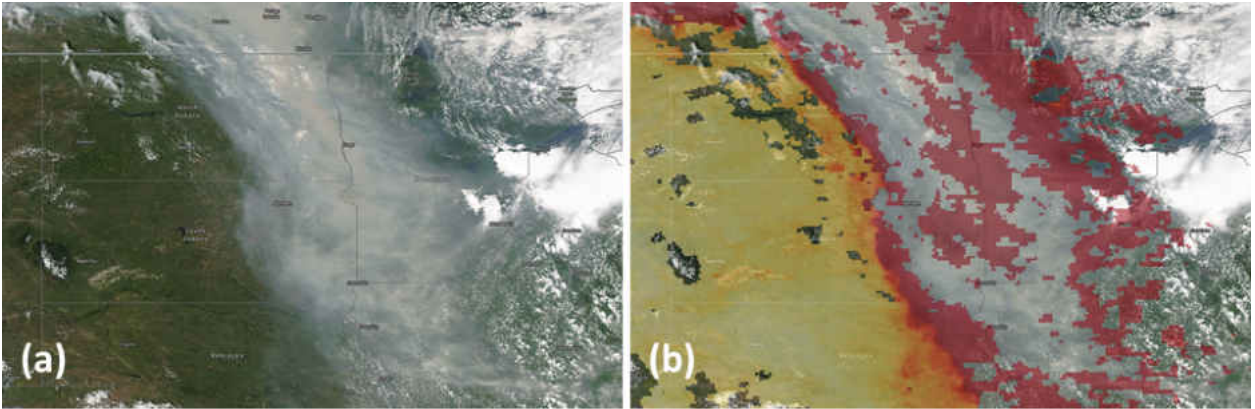


Figure 9: **(a)** Aqua MODIS imagery for 29 June 2015 at $\sim 19:30$ UTC. **(b)** as (a) but with overlaid AOD values. Yellows indicate lower AODs (less than 1.0) while reds indicate higher (greater than 1.0). Unshaded areas indicate regions without aerosol or thick smoke plumes that are misclassified as cloud by the MODIS aerosol retrieval algorithm. From NASA Worldview.

One noticeable difference between the NAAPS and WRF-Chem simulations is the magnitude of the smoke plume. The NAAPS simulation shows a maximum AOD of ~ 2.5 in western Manitoba, whereas the WRF-Chem simulation indicates a band of higher AOD near ~ 3.5 extending from western Manitoba nearly to Fargo, North Dakota. In addition, a higher AOD of ~ 2.0 exists in western Ontario in the WRF-Chem simulation, while the NAAPS simulation indicates an AOD of ≤ 1.0 for the same area. This increased AOD can possibly be attributed to boundaries ingesting NAAPS data every three hours as well as convergence over the Red River Valley region. Thus, while the structure of the plume is similar in both models, the magnitude is higher in the WRF-Chem simulations. Note, the Grand Forks

AERONET site reported an AOD value (500 nm) of ~ 3.7 on 29 June at 15Z. AOD values are ~ 3.0 and ~ 2.0 at 15 UTC in the Grand Forks area for the WRF-Chem simulation and NAAPS analysis, respectively.

As expected, the model simulated smoke plume (Figure 8c and f) on 29 June at 18Z is more consistent with the smoke plume as observed at about 19:30Z by the Aqua MODIS (Figure 9). NAAPS and WRF-Chem demonstrate regions with AODs larger than 1.0 extending further into eastern South Dakota, southern Minnesota, and the northwestern corner of Iowa. As previously discussed, the smoke plume was most significant at this time in Grand Forks, ND. In Grand Forks, NAAPS and WRF-Chem indicate AODs of ~ 3.0 for the 18Z time while observations from AERONET had an AOD (500 nm) of around 4.5.

5.2 Impacts to Surface Downward Shortwave Radiation

The presence of smoke plumes should decrease downward shortwave radiation that reaches the surface through the scattering and absorption of solar energy (i.e., through the aerosol direct effect). Such an effect is evident in the WRF-Chem simulations as shown in Figure 10. Figure 10a and b show the simulated surface downward shortwave radiation, or SW flux, at 18 UTC for 29 June 2015 from the WRF-Chem control and chemistry simulations, respectively.

Higher and relatively uniform SW flux values of around $800\text{-}1000 \text{ Wm}^{-2}$ are found throughout the domain for the control simulation (except for speckled areas of cumulus cloud; Figure 10a). In comparison, SW flux values of around 800 Wm^{-2} or less are found outside of the dense smoke plume in the chemistry simulation, while much lower SW flux values of $\sim 400 \text{ Wm}^{-2}$ are found within the dense smoke plume (Figure 10b). Furthermore, while both the control and chemistry simulations have low SW flux values in the eastern portion of the domain associated with cumulus

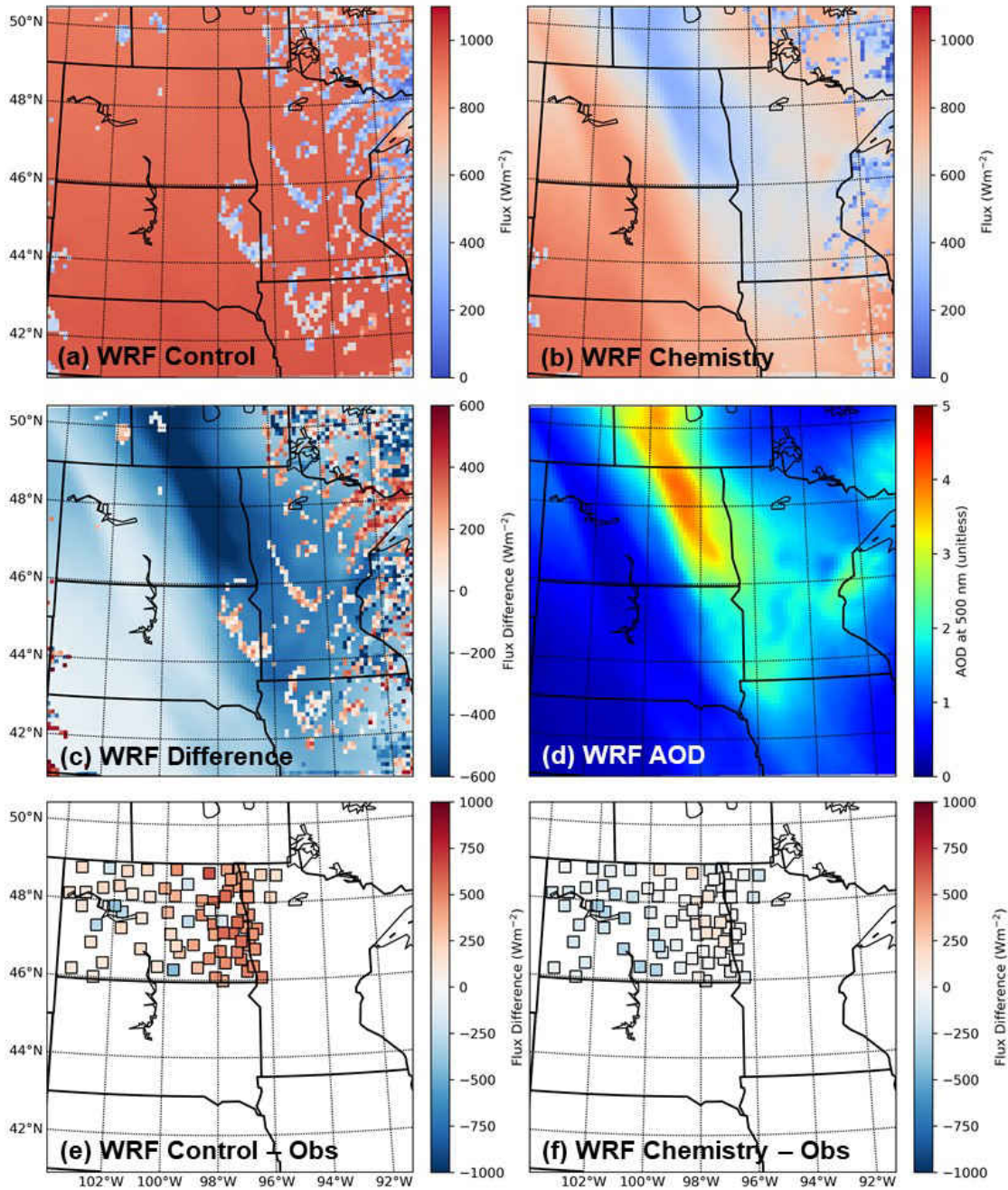


Figure 10: (a) SW flux for 29 June at 18Z from the WRF-Chem control simulation. (b) as in (a) but for WRF-Chem chemistry simulation. (c) Difference in SW flux between WRF-Chem chemistry and control runs where reds indicate more SW reaching the surface in Chemistry run and blues indicate less SW reaching the surface in the Chemistry run compared to Control. (d) AODs from WRF-Chem chemistry run for 29 June at 18Z. (e) Differences in SW flux between Control simulation and NDAWN observations where reds indicate Control simulation SW was higher and blues indicate Control simulation SW was lower than NDAWN observations. (f) as in (e) but for Chemistry simulation.

clouds, areal extent and frequency of these clouds are lower over Minnesota, South Dakota, Manitoba, and Saskatchewan in the chemistry simulation. This may suggest that the smoke plume could be inhibiting cumulus cloud production (e.g., Ackermann et al., 2000; Koren et al., 2004). However, the impacts of aerosol on cloud formation is not the focus of this study.

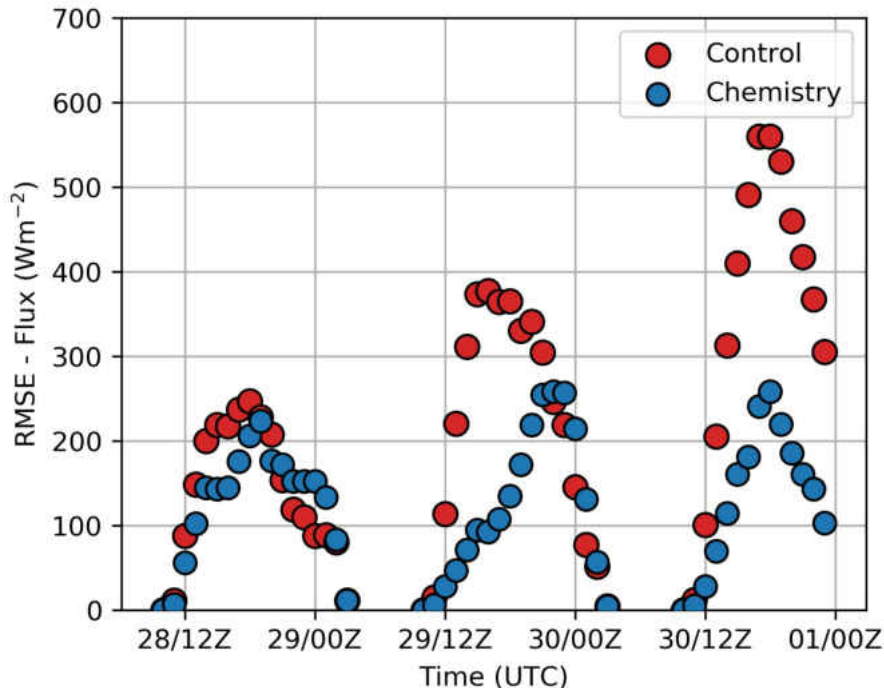


Figure 11: RMSEs of surface downward shortwave flux (SW flux) from WRF-Chem throughout the 72-hr WRF-Chem simulations. The left-hand axis indicates RMSE with red dots being for the control simulation and blue for the chemistry simulation. A total of 75 NDAWN stations are used to calculate the values for each time step.

Figure 10c shows the SW flux differences between the chemistry and control simulations. As expected, much less SW flux reaches the surface in central and eastern North Dakota where the smoke plume is predicted in the chemistry simulation where the control simulation SW flux in this area is $\sim 950 \text{ Wm}^{-2}$ and the chemistry simulation is $\sim 350 \text{ Wm}^{-2}$ for the same approximate area. Thus, also as expected, the maximum difference of $\sim 600 \text{ Wm}^{-2}$ in SW flux is found over regions with dense

smoke, as indicated in Figure 10d. These SW flux differences are, again, clearly seen by comparing the model simulations with surface-based observations from NDAWN data as shown in Figure 10e and f. The WRF-Chem control simulation overestimates the SW flux on the order of 500 Wm^{-2} over the smoke aerosol polluted regions. While this overestimation in SW flux is much reduced for the WRF-Chem chemistry simulation, a slight overestimation still exists ($< 250 \text{ Wm}^{-2}$; Figure 10f) likely due to the WRF-Chem underestimation of aerosol loading or inherent uncertainties in the aerosol optical models.

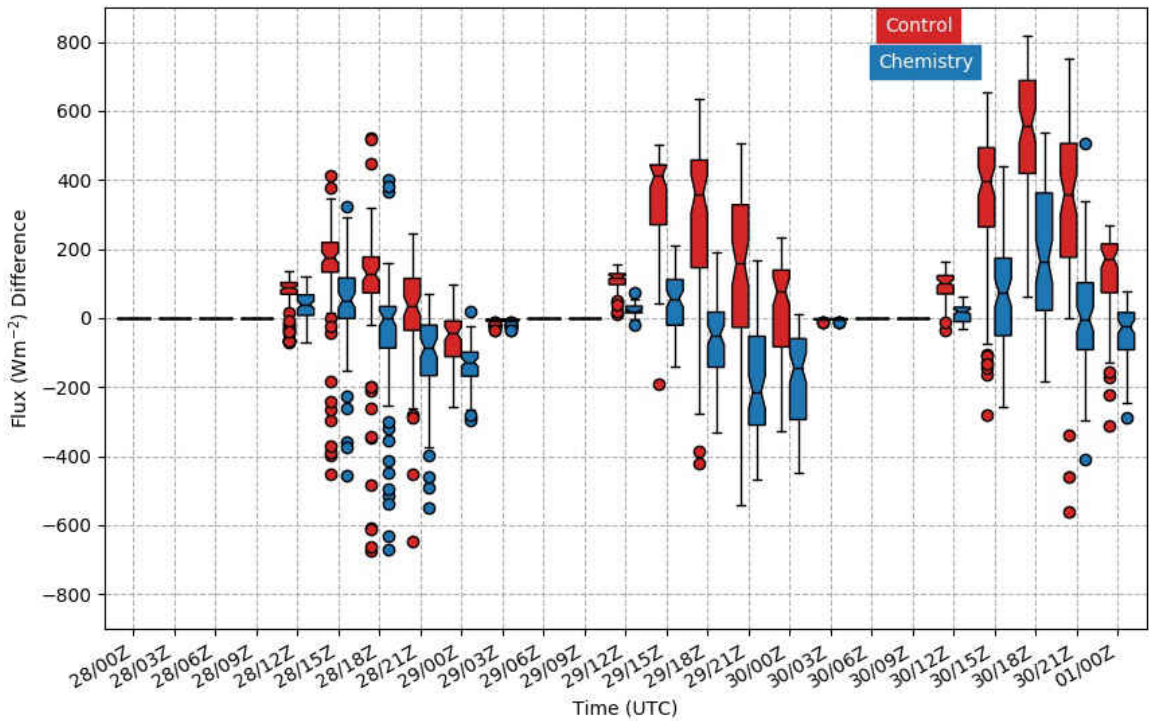


Figure 12: Box and whiskers time series plot for SW flux analysis minus observation differences. Red represents the WRF-Chem control simulation and blue represents the WRF-Chem chemistry simulation. Dots represent data outliers for that time.

Figure 11 shows the RMSE time series of SW flux estimated from both WRF-Chem control and chemistry runs by comparing WRF-Chem simulated SW flux with observations from the NDAWN surface stations. On 28 June, similar RMSE values of

SW flux are found for both the control and chemistry simulations. However, daytime RMSE values improve by nearly 100 Wm^{-2} on 29 June and almost 300 Wm^{-2} on 30 June for the chemistry simulation. Although this plot is only indicative of NDAWN surface stations in and near North Dakota, this bodes well for the remainder of the domain since NDAWN stations range from areas completely under the smoke plume directly to areas with little aerosol loading.

To further illustrate the performance of model simulated SW flux, Figure 12 shows the box and whiskers plot for SW flux differences between analysis and observations for each model output time. The control simulation consistently has a higher bias in SW flux compared to the chemistry simulation be about 200 Wm^{-2} . The chemistry simulation tends to have a low bias, indicating SW flux simulations tends to be underestimated compared to the NDAWN observations.

5.3 Impacts to Surface Temperature

The impacts of aerosols on WRF-Chem simulated surface temperatures are shown in Figure 13. With the downscaling of NAAPS aerosol data, the temperature fields from the chemistry simulation at 18Z on 29 June agree reasonably well with observed temperatures beneath the smoke plume as seen in Figure 13f. The WRF-Chem control and chemistry-simulated temperatures disagree most where the chemistry run reported the highest AOD values (Figure 13e and f, respectively), while areas with negligible AOD values have minimal temperature differences between the control and chemistry runs (e.g., western South Dakota and western Nebraska). In comparing with the surface-based temperature observations as shown in Figure 13e, larger temperature biases on the order of 5.0°C are found over dense smoke regions for the control run. These biases are largely reduced with the inclusion of NAAPS aerosol fields in the chemistry run, as shown in Figure 13f.

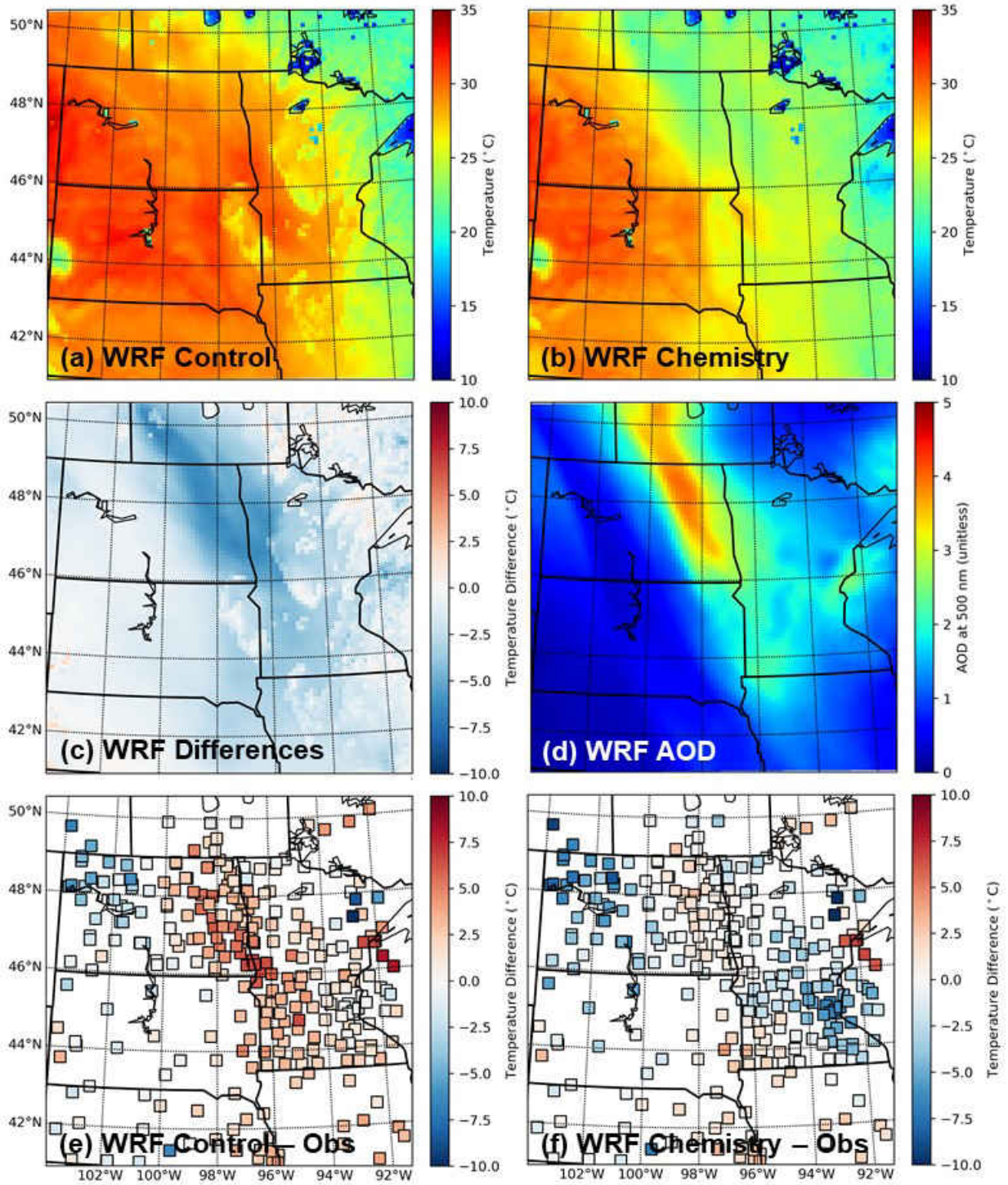


Figure 13: As with Figure 10, but for 2m temperature. Observations included in (e) and (f) are from both ASOS and NDAWN station datasets.

It is interesting to find that the maximum temperature bias for the control simulation occurs before sunset each day during the smoke event, as suggested in Figure 14. Figure 14 shows both the control and chemistry simulation time series of the averaged RMSE for temperature from 00Z, 28 June to 00Z, 01 July evaluated against NDAWN and ASOS surface observations in the study region. The daily peak RMSE is found around 00Z each day for the control run with the maximum RMSE in temperature reaching nearly 5.0°C. In comparison, peak RMSE values for chemistry simulation 2m temperature are approximately 1.0°C lower than the control run (i.e., near 4.0°C) at 20Z on 28 June and decrease to near 3.5°C at 20Z on 30 June.

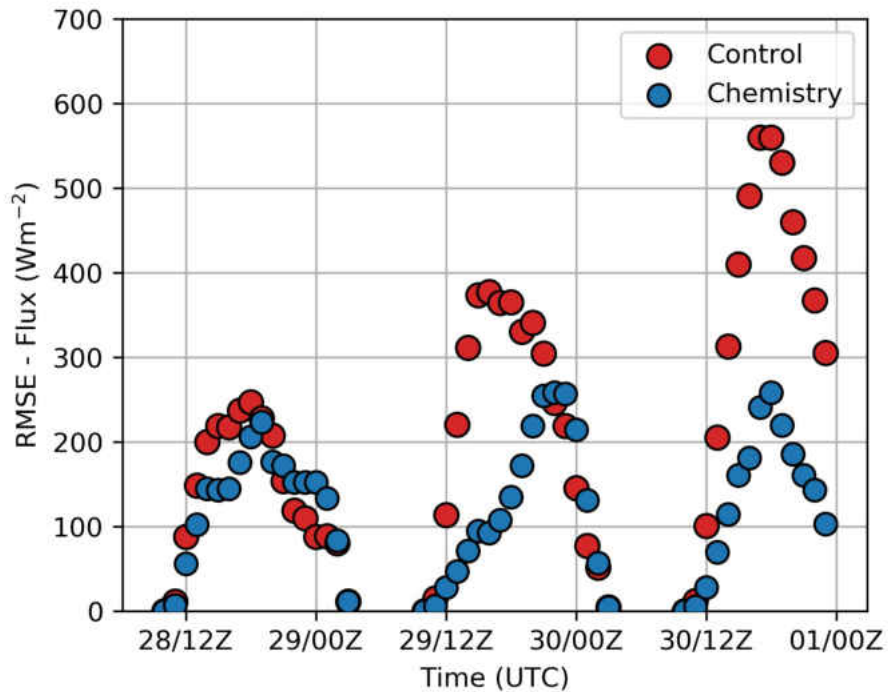


Figure 14: Similar to Figure 11 but for 2m temperature. The right-hand axis and green bars indicate the number of observations used to calculate the RMSE for that time.

The box and whiskers plot for 2m temperature analysis minus observation differences (Figure 15) indicates mean control temperatures at the majority of WRF-

Chem model time steps are warm-biased by 1-3°C compared to temperature observations. This warm-bias in the control simulation increases as heavier smoke moves into the study region. In contrast, the chemistry simulation mean temperature tends to be cold-biased, although at a smaller magnitude than the control simulation’s warm-bias.

About one and a half hours after sunrise, the control run has nearly no bias whereas a large cold bias of nearly 2.0°C (Figure 15) occurs in the chemistry simulation at 12Z on 30 June. It is hypothesized that the lack of aerosol in the control simulation allows the maximum temperature to reach a higher maximum later in the day compared to the chemistry simulation. Consequently, this causes the control run minimum temperatures overnight to be closer to observations than the chemistry simulation.

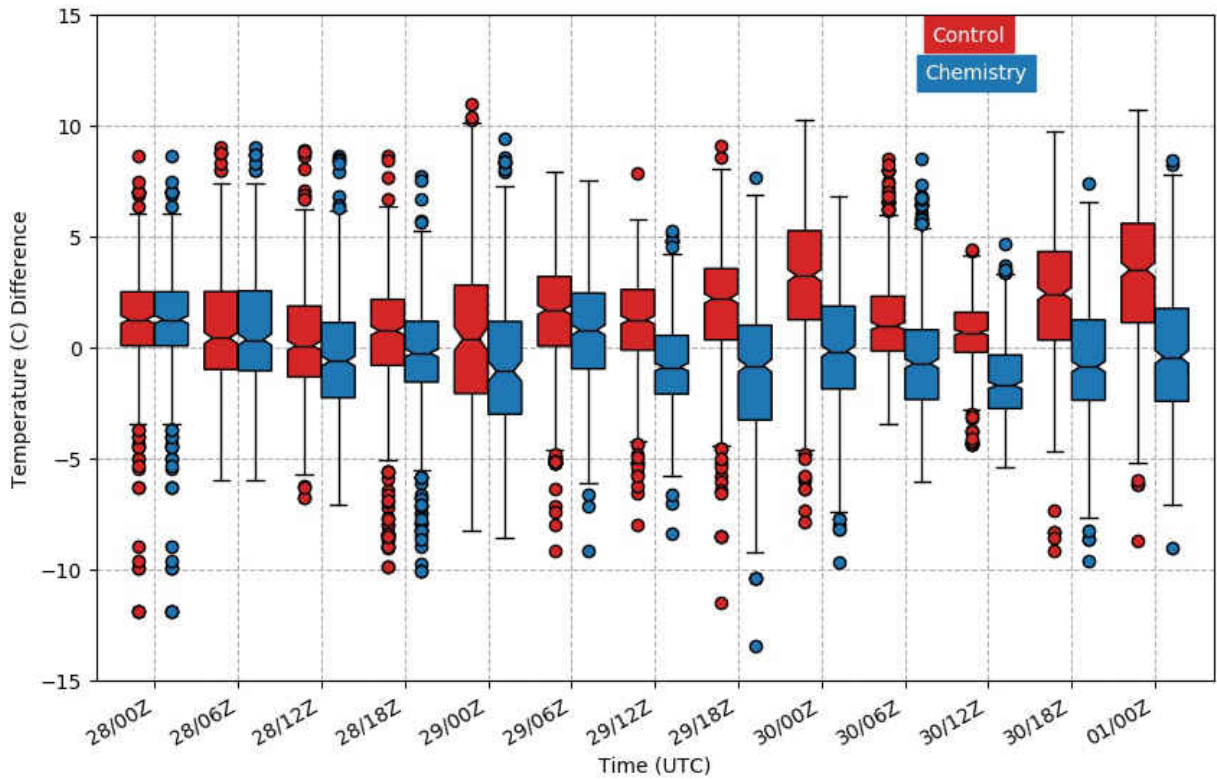


Figure 15: As in Figure 12 but for 2m temperature.

5.4 Impacts to 10m Wind Speeds

The 10m wind speeds are analyzed for differences between control and chemistry simulations and, then, compared to ASOS observations. Note that NDAWN surface wind observations are not included because observations are not required to be recorded at 10m. The most noticeable difference occurred 29 June at 18Z (i.e., Figure 16) where the magnitude of differences in winds for the chemistry run are very slightly closer to

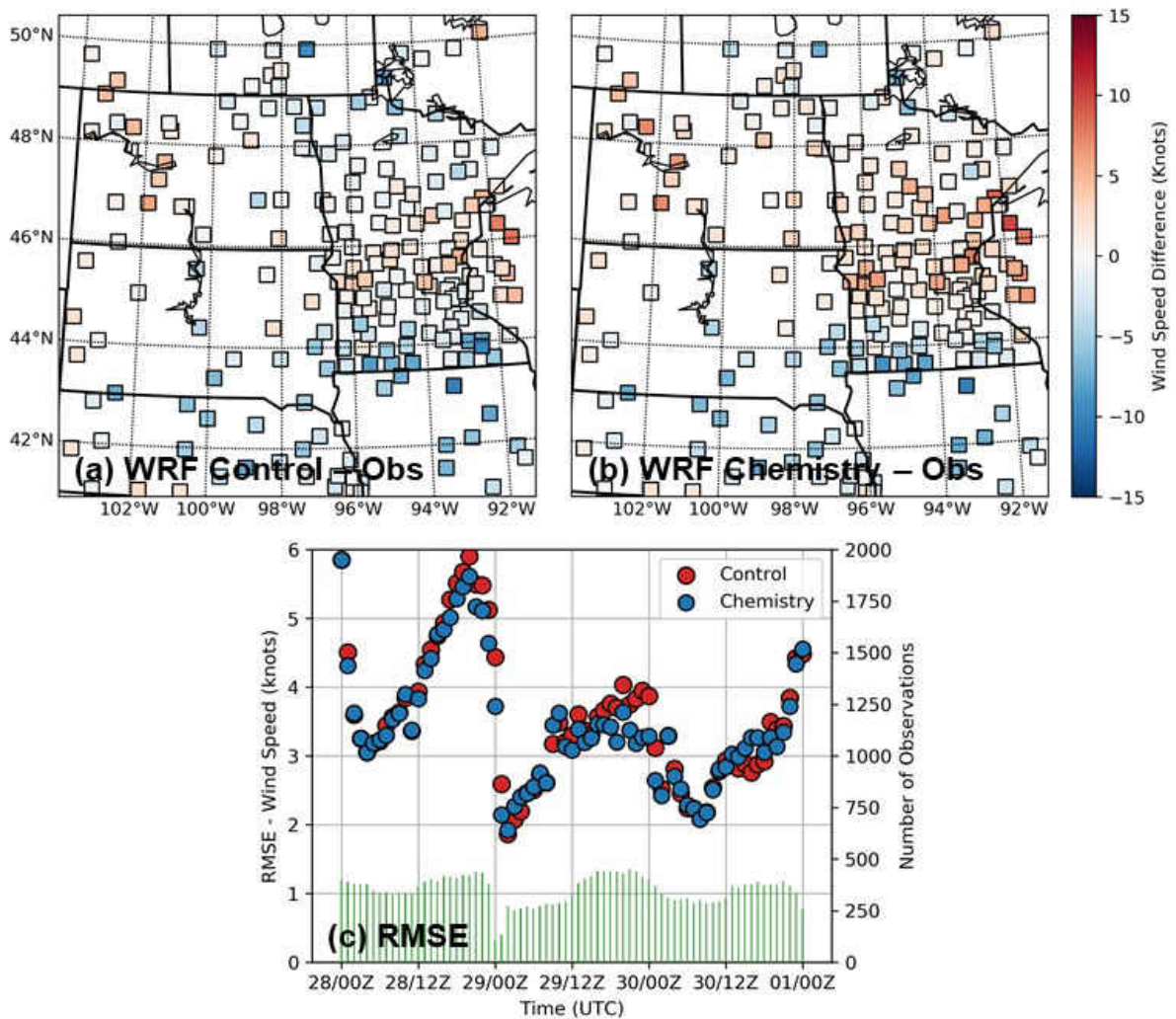


Figure 16: Difference in 10m wind speed between (a) WRF-Chem control simulation and observations from ASOS stations and (b) as in (a) but for chemistry simulation. (c) Similar to Figure 11 and Figure 14 but for 10m wind speed.

observations in the Red River Valley and northern and central Minnesota compared to the control run. This may be attributed to the lower surface temperatures reducing momentum flux and preventing the typical summer thermals that would otherwise create wind. Aside from the slight improvement to chemistry-simulated wind speeds on the afternoon of 29 June, there is not a particularly apparent pattern in wind speeds.

Figure 16c shows the RMSE for wind speed of both control and chemistry simulations evaluated against ASOS 10m wind speed observations. Minor differences in the RMSE of wind speed are found between the simulations and observations, although the largest RMSE differences are found in the afternoon of 29 June and are only on the order of 0.5 knots.

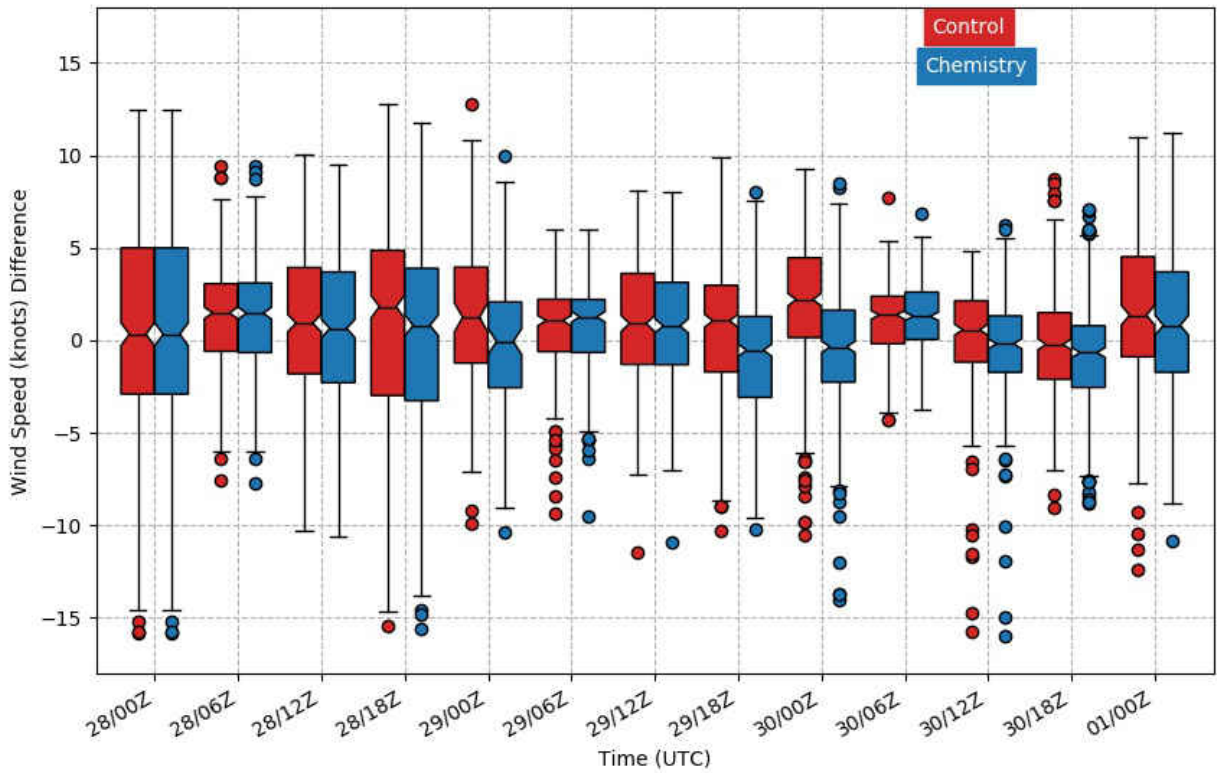


Figure 17: As in Figure 12 and Figure 15 but for 10m wind speed.

For the control simulation, mean wind speed tends to be biased high – particularly in the afternoons – and the chemistry simulation is generally biased high except for early afternoon when wind speeds are biased low (Figure 17). However, it’s important to note that the maximum bias is about 2.0 knots, a low bias especially considering wind observations less than 2.5 knots are considered light and variable. Thus, the numerical model simulated wind fields may be less impacted by the presence of smoke plumes, but further case studies are necessary to fully evaluate.

5.5 Impacts to Planetary Boundary Layer Height

The planetary boundary layer (PBL) is the lowest portion of the atmosphere where Earth’s surface can impact meteorology through heating, friction (via the Earth’s surface, buildings, trees, mountains, etc.), and turbulence mixing. In general, the PBL height is maximized during the day due to shortwave radiation warming the Earth’s surface and causing convective turbulence within the PBL. Conversely, PBL heights are minimized at nighttime due to the lack of solar radiation at night allowing the boundary layer to stabilize via radiative cooling (Stull, 1988).

As expected, the simulated PBL reaches maximum height during the day in both simulations. However, without as much solar shortwave radiation reaching the surface, the chemistry simulation (Figure 18b) experiences less convective turbulence from the decreased temperatures compared to the control simulation (Figure 18a). As a result, the area beneath the smoke plume in the chemistry simulation has lower maximum PBL heights than the control simulation. In Figure 18c, the largest differences between the control and chemistry simulations for 29 June 2015 at 18Z occur where AOD values are highest (Figure 18d). The PBL heights of the control simulation are nearly 2 km higher than the chemistry simulation’s approximate 500 m maximum PBL heights in this region. Outside of the smoke plume, the chemistry

simulation is closer to the control simulation with PBL heights of about 1 km, and higher in the western edge of the domain where the terrain becomes mountainous due to the Rocky Mountains.

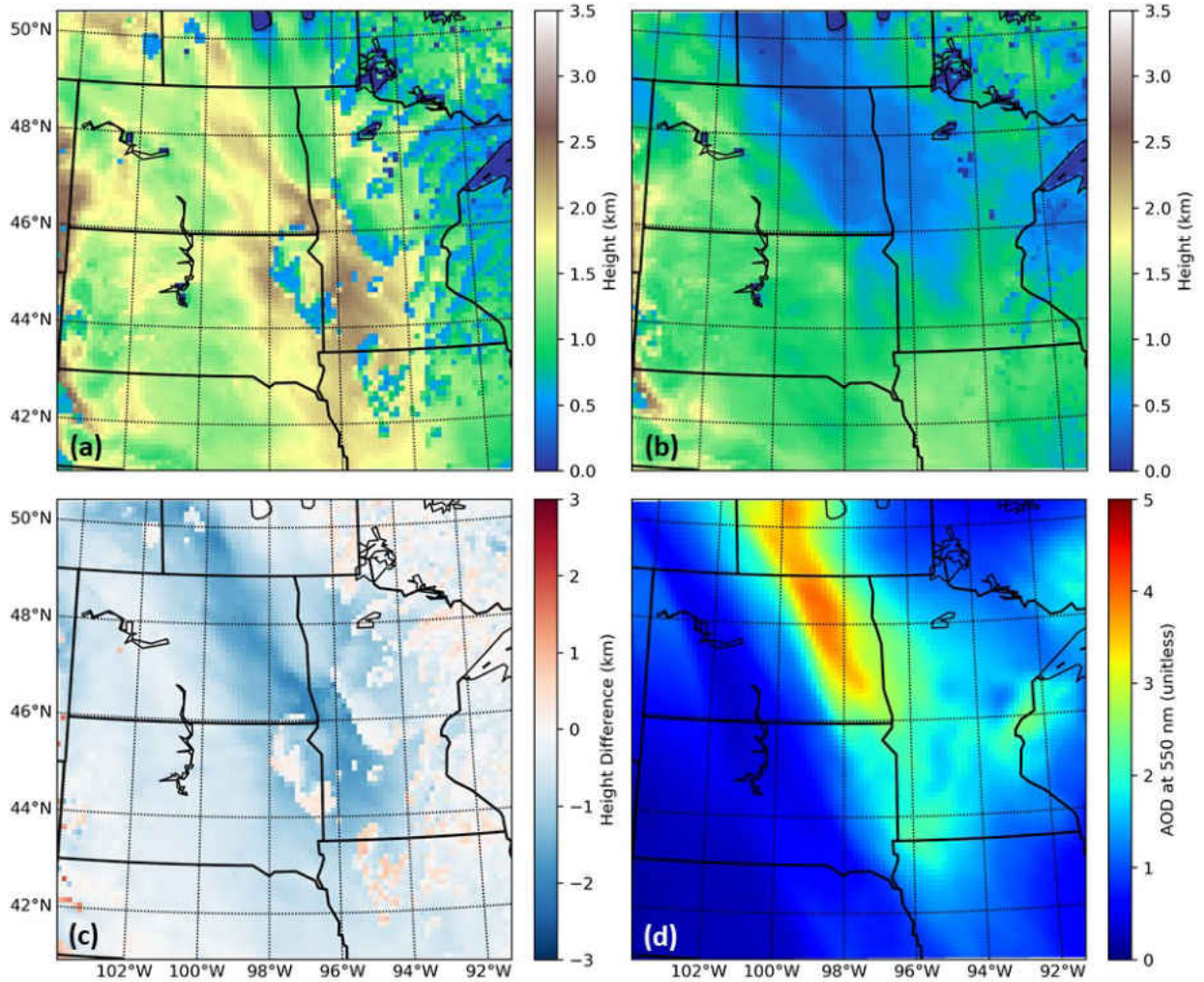


Figure 18: (a) PBL heights for WRF-Chem control simulation on 29 June at 18Z, (b) as in (a) but for chemistry simulation, (c) difference plot of chemistry minus control simulations where red areas indicate the chemistry simulation has higher PBL heights and blue areas indicate the chemistry simulation has lower PBL heights compared to the control simulation, and (d) WRF-Chem AOD for reference.

As expected, PBL heights for the control and chemistry simulations are in good agreement during the nighttime. Differences between the simulations are on

the order of 100 m, such as in 30 June at 03Z (i.e., 10 pm CDT) as opposed to the kilometers of differences during the day. Even with the smoke plume being nearly at its most intense, the PBL heights are minimally affected since solar radiation is one of the main drivers for PBL height evolution.

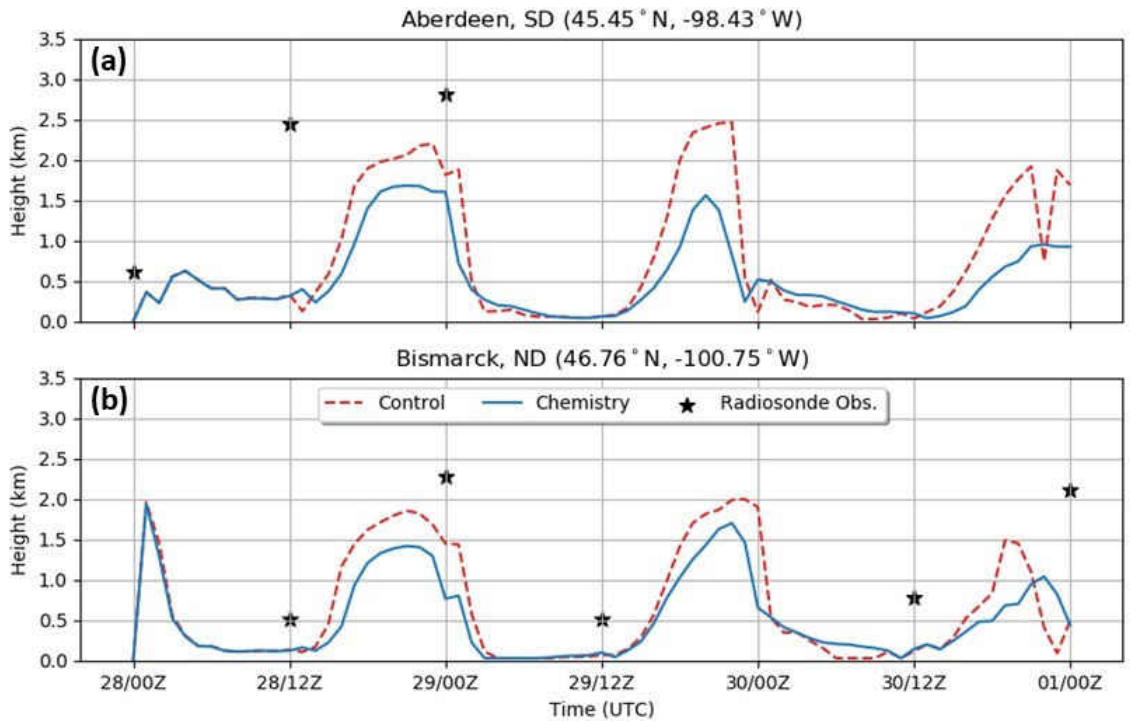


Figure 19: (a) Aberdeen, SD PBL heights throughout the WRF-Chem 72-hr simulations. The control simulation is represented by the dashed orange line, the chemistry simulation represented by the solid blue line, and radiosonde derived PBL height observations are indicated by the black stars. (b) as in (a) but for Bismarck, ND

It is difficult to validate PBL height model performance because radiosonde balloon launches are spatially and temporally limited being only launched twice daily (00Z and 12Z) at select locations across the United States. PBL height observations require meteorological data from a variety of altitudes that surface observation stations cannot reach. As a result, the smoke plume's trajectory during the smoke event aligned poorly with existing balloon launch locations— only two balloon launches occurred during the event in the vicinity of the smoke plume (Bismarck, North Dakota

and Aberdeen, South Dakota). While these locations are on the edge of the smoke plume, Aberdeen did have a MODIS-indicated AOD of ~ 2.0 (Zhang et al., 2016).

Observed PBL heights are calculated by locating a virtual potential temperature gradient increase of 2.0 K with a minimum gradient in that layer of 0.5 K per 100 m (Schmid and Niyogi, 2012). PBL heights as seen in Figure 19 for Aberdeen, SD (a) and Bismarck, ND (b) follow the typical PBL height evolution pattern with the highest PBL heights occurring during the day and lowest occurring at night. However, the calculated PBL height from the surface observations are different from simulations from either the control or the chemistry runs. This may be caused by the inherent limitations of accurately simulating PBL heights with NWP models through PBL schemes.

5.6 Forecast Sensitivity Study

A sensitivity study is also conducted to analyze the effect of aerosols on short-range forecasted SW flux, temperature, and, wind fields. To achieve this goal, the archived NAM forecasts, instead of NAM analyses, are used as the initial and boundary conditions for WRF-Chem simulations. As discussed in Chapter 4, NAM Analysis data is generated through assimilation of observations, whereas the NAM forecast data is simply the NAM analysis integrated forward in time. NAM forecast data allows for an evaluation of the smoke plume's influence on the meteorological forecast as if it were occurring in real time from a simulated operational environment. Note that while the NAAPS forecast may be used in an operational environment, here the study is limited to NAAPS analysis as a means of ensuring a better representation of the smoke plume.

Furthermore, it is assumed that NAAPS aerosol forecasts are the same as NAAPS aerosol analyses as used in the study, although larger uncertainties are ex-

pected for NAAPS forecasts. By using NAM forecasts as the initial and boundary conditions, the “operational forecast” scenario is simulated, and herein refer to the WRF-Chem runs as WRF-Chem forecasts. A total of five WRF-Chem 48-hour forecasts runs initiated at 00, 06, 12, 18 UTC on 28 June 2015 and 00 UTC on 29 June 2015 are examined in this section.

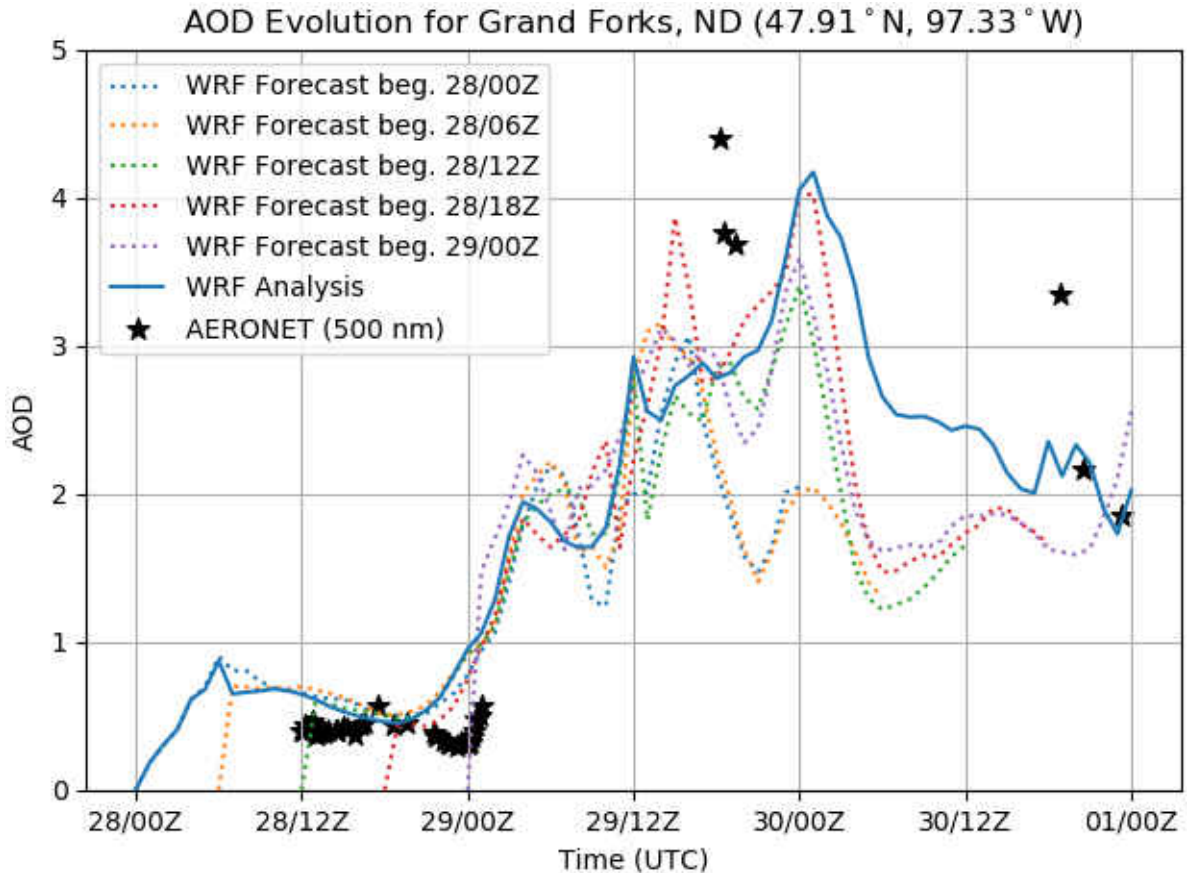


Figure 20: AOD as observed by AERONET (500 nm; black stars) and WRF-Chem simulations (550 nm) initialized with NAM Analysis data (solid line), and NAM forecast data (dotted lines).

Ground-based AOD data are available at the Grand Forks AERONET station throughout the smoke event. Thus, the WRF-Chem modeled AOD for the five WRF-Chem forecast runs over Grand Forks, ND are shown in Figure 20. Also included are AODs from the WRF-Chem analysis run for Grand Forks, ND and AODs recorded

by the Grand Forks, ND AERONET during the study period. Large gaps in recorded AERONET data may be caused by several factors. For one, AERONET can only record data in cloud-free daylight conditions. Another possibly cause for data gaps is the smoke plume having been so optically thick that it was misclassified as cloud by the AERONET.

While general patterns are similar, AODs for the five forecasting runs diverge from about 12 UTC on 29 June 2015 until 05 UTC on 30 June. In addition, AODs from forecast runs during this period are mostly lower than the AODs of the analysis run. Yet, AERONET data are more consistent with AODs from the analysis run. AOD patterns from later forecast times of the five WRF-Chem forecast runs – namely for forecast runs initialized at 12 and 18 UTC on 28 June and 00 TUC on 29 June – are closer to the AOD pattern from the WRF-Chem analysis run. This may indicate that more accurate forecasts are expected for a shorter forecasting period. It is also worth noting that NAAPS data assimilation is limited to daytime observations due the use of MODIS AOD product (Lynch et al., 2016).

RMSE statistical analysis was performed on surface observations co-located with WRF-Chem SW flux simulations to determine improvements to the WRF forecast. Figure 21 shows the RMSE time series of SW flux for each of the NAM forecast 48-hour simulations with the first initialization beginning 28 June at 00Z and the last initialization beginning 30 June at 00Z. The first model time step is excluded from analysis here because the SW flux is 0.0 Wm^{-2} domain-wide at initialization regardless of time of day. Figure 21a shows the time series for the control simulations, while Figure 21b shows the chemistry simulations. In general, there are minimal differences in RMSE at any one time in the control simulations despite the varied initialization times. This pattern is also present in the chemistry simulations, although there is slightly less agreement in RMSE between 28 June at 12Z and 29 June at 00Z. Both

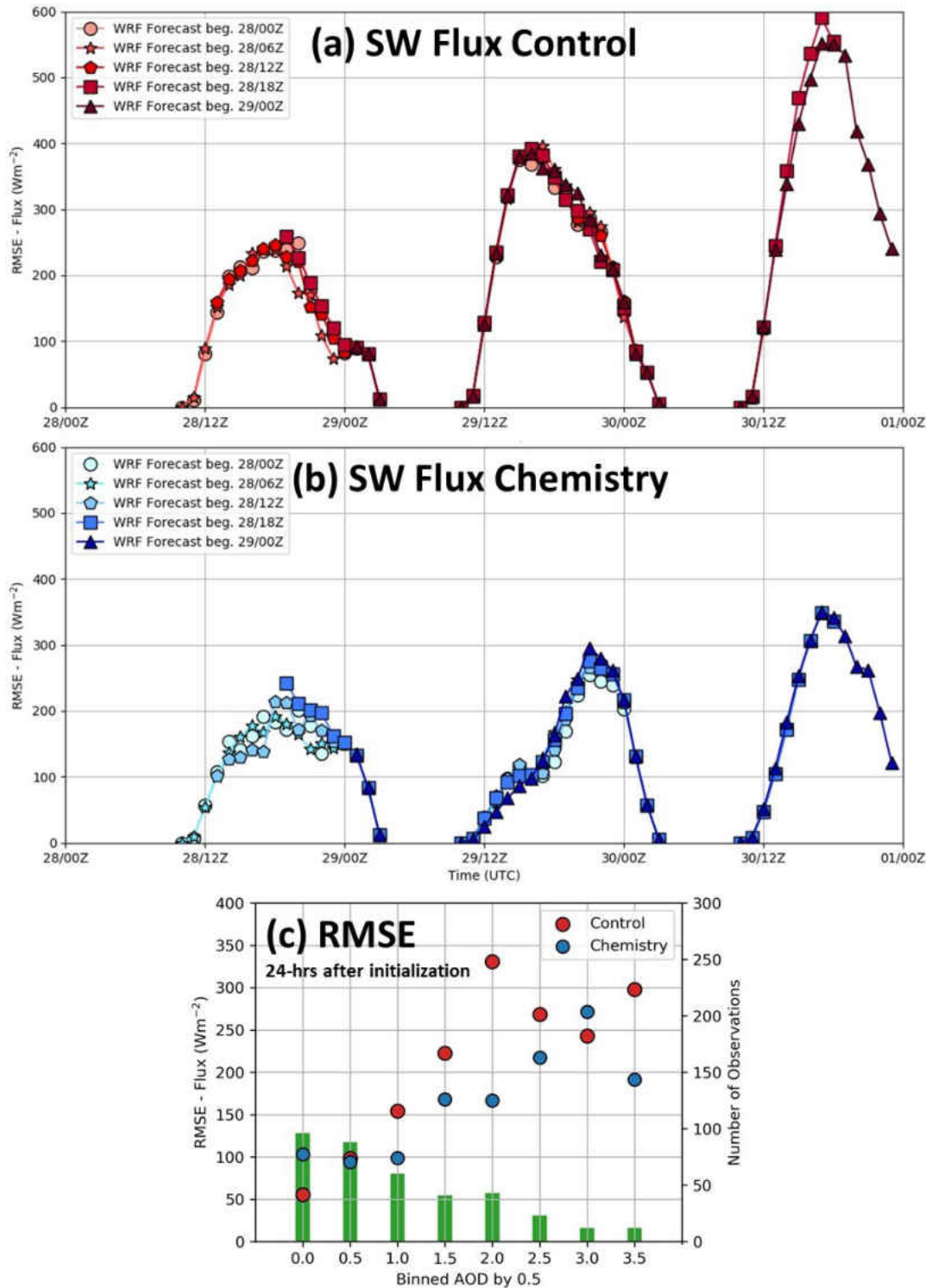


Figure 21: (a) RMSE time series of SW flux for each of the five WRF-Chem Control simulations. Each run is denoted by a different symbol and color shade. (b) Same as (a), but for Chemistry simulations. (c) RMSE of SW flux 24 hours after initialization for all WRF-Chem simulations binned by AODs of 0.5.

the control and chemistry simulations for the WRF-Chem runs initialized on 28 June at 18Z and 29 June at 00Z include outliers at the beginning of the forecasts. Because this feature occurs in both control and chemistry simulations, it is most likely due to initialization occurring at or after sunset. Still, it remains evident that aerosol inclusion minimizes the RMSEs of simulated SW flux when comparing control and chemistry simulations regardless of initialization time.

Figure 21c shows the bin-averaged RMSEs of SW fluxes 24 hours after initialization as a function of AOD for both control and chemistry runs. RMSEs are binned for every 0.5 AOD. In general, chemistry simulations have lower RMSEs for SW flux compared to control for most bins. However, there are several exceptions to this where the control RMSE is slightly lower than the chemistry: the 0.0-0.5 AOD bin and the 3.0-3.5 AOD bin. These unexpected examples of seemingly poorly simulated SW flux likely have several causes. For one, AODs are slightly overestimated in the western portion of North Dakota, thereby causing lower SW fluxes than observations. The SW flux is also at or near 0.0 Wm^{-2} during nighttime even when AODs are significant (i.e., greater than 1.0). Furthermore, simulated clouds can bias the SW flux and cause differences between control and chemistry simulation RMSEs.

Figure 22 shows the RMSE time series and as binned by AOD for 2m temperature similar to Figure 21 for SW flux. Chemistry run temperatures (Figure 22b) generally have lower RMSEs than the control simulations (Figure 22a) – as is expected from the lower RMSEs in the SW flux for chemistry simulations. RMSEs for a particular time tend to be lowest for the later forecasts (e.g., for both control and chemistry simulations, the lowest RMSEs between 00Z to 12Z on 30 June come from the forecasts initialized on 29 June at 00Z). Still, the control RMSEs are mostly lower than chemistry overnight on 30 June for all forecasts. Again, this may be attributed

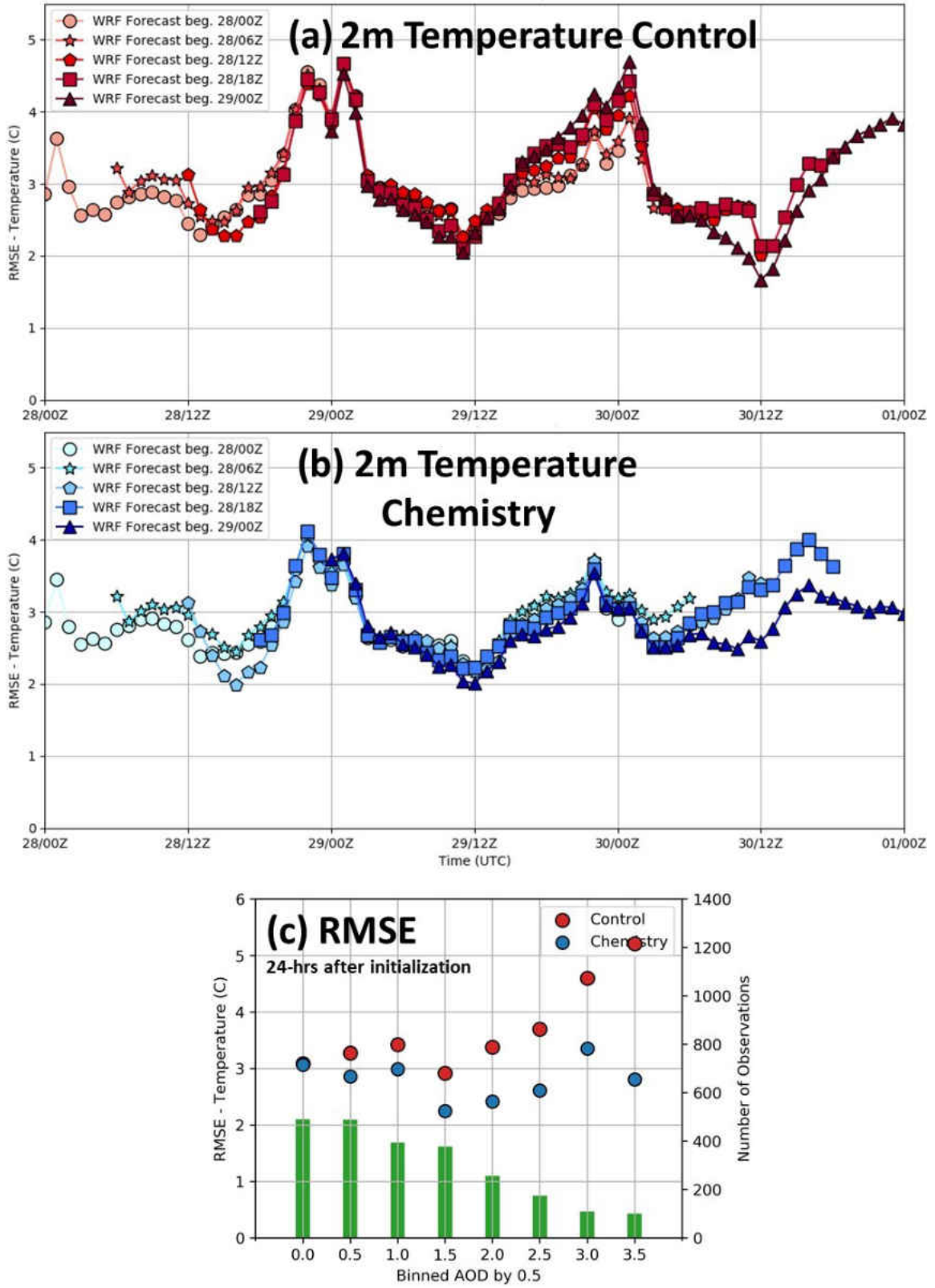


Figure 22: As in Figure 21, but for 2m temperature.

to the minimization of the diurnal heating cycle in the chemistry run due to the presence of aerosol that causes nighttime temperatures to be lower than observations.

RMSEs from chemistry runs are lower for all other AOD bins (Figure 22c). In fact, the difference in RMSE between control and chemistry increases with increasing AOD. The largest difference is seen in the bin for AODs ≥ 3.5 with the control RMSE being over 5°C and chemistry at less than 3°C for an overall difference of greater than 2°C . In addition, the chemistry RMSEs are never greater than 3.5°C . This suggests that the SW flux is less biased prior to 24 hours after initialization than the RMSE values otherwise indicate.

Wind speed RMSEs for chemistry (Figure 23b) are generally similar to or lower than the control simulations (Figure 23a) – most notably on 29 June between 12Z and 00Z. Similar to temperature, the later initialized forecasts tend to have lower RMSEs for both the control and chemistry simulations. However, the largest difference between control and chemistry occurs on this afternoon. Control simulations peak with RMSEs of 6 knots or greater, whereas the chemistry simulations for the same time period peak with RMSEs of about 4.5 knots. This suggests the lower surface temperatures result in less turbulent mixing, as previously discussed. Similar to the surface temperature, 10m wind speeds tend to be better forecasted by the model simulations initialized later. Finally, Figure 23c shows wind speed RMSEs for 24 hours after initialization as binned by 0.5 AOD. The RMSEs from chemistry runs are less than the control RMSEs for all AOD bins. As the AOD increases, the differences between the control and chemistry simulation RMSEs increase as well – reaching ~ 1.0 knot for the bin of AODs ≥ 3.5 . This may be related to the control simulation’s overestimation of surface temperatures as the AOD increases causing increased turbulent mixing that overestimates wind speed.

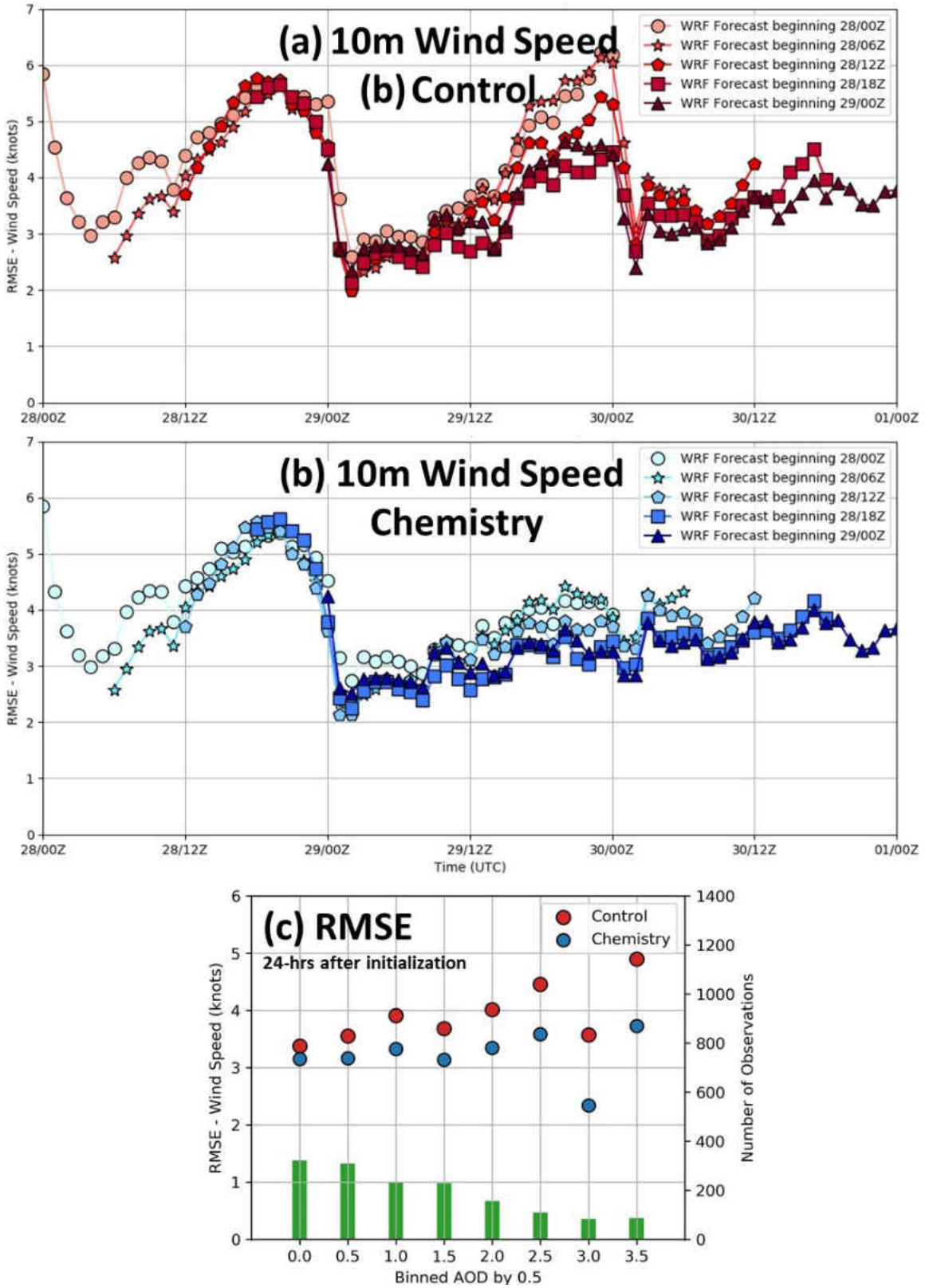


Figure 23: As in Figure 21 and Figure 22, but for 10m wind speed.

In summary, improvements are found in forecasted SW flux, near-surface temperature, and near-surface wind speed 24 hours after initialization with the dynamical downscaling of NAAPS data into WRF-Chem. This finding further proves that NWP analysis and forecast can be improved through dynamical downscaling of CTM data for heavy aerosol events.

CHAPTER 6

CONCLUSIONS

Studies have shown that through attenuation of solar radiation and absorption of outgoing longwave energy, atmospheric aerosols can directly affect meteorological phenomena on regional weather scales (e.g., Zhang et al., 2016). To account for the impacts of aerosols on weather, research has been conducted for incorporating aerosols into numerical weather prediction (NWP) models. Still, while the impacts of heavy aerosol plumes on weather have been reported, it remains a scientific debate as to whether clock time is ultimately wasted by incorporating aerosols in numerical forecasts for regions and seasons with low aerosol loadings.

In this study, an alternative approach is attempted through dynamically downscaling aerosol analyses and forecasts from a global chemical transport model (CTM) into an NWP model for improving the accuracy of weather forecasted near-surface meteorological properties. This concept is tested through downscaling of NAAPS aerosol analyses into the WRF-Chem model for the June – July 2015 biomass burning aerosol episode over the Northern Great Plains. NAAPS aerosol data is used as initial and boundary conditions for aerosols with NAM analyses and forecasts used as initial and boundary conditions for meteorological fields. This study finds:

1. **Surface downward shortwave radiation (SW flux) is significantly over-estimated during the daytime without the consideration of solar attenuation by aerosol plumes.** The RMSE of SW flux is found to be ~ 300 Wm^{-2} higher for the control run as compared to the chemistry run at 18 UTC

on 30 June 2015. This result is not surprising since the presence of optically thick smoke aerosol plumes can significantly reduce SW flux.

2. **Noticeable reductions in the RMSE of temperature analyses and forecasts when aerosol fields are incorporated into the model through dynamical downscaling of NAAPS aerosol data as compared with the control simulations (i.e., WRF-Chem simulations without inclusion of aerosol fields).** For example, the RMSE in WRF-Chem forecasted temperature increases from $\sim 3.0^{\circ}\text{C}$ in the chemistry simulation (i.e., WRF-Chem simulations using NAAPS aerosol data as initial and boundary conditions) to more than 5.0°C in the control simulation for locations where WRF-Chem forecasts an $\text{AOD} \geq 3.5$.
3. **Large reductions in planetary boundary layer (PBL) height are also found with the inclusion of aerosol in WRF-Chem simulations.** While surface observations are unavailable for estimating PBL height near the center of the smoke plumes, radiosonde data from Bismarck, North Dakota and Aberdeen, South Dakota (both of which were at the edge of the thick smoke plume during this smoke event) found that neither the control nor the chemistry simulations can simulate PBL heights with much accuracy.
4. **Marginal impacts to wind speed due to inclusion of aerosols can be seen in the WRF-Chem simulated wind speeds.** RMSE of chemistry simulated wind speed decreased by nearly 1.0 knot compared to the control simulation. Still, it is worth noting that this was not a high wind event.

While only a single case, this study demonstrates the new concept of incorporating the impact of aerosols on NWP model forecasts. Compared with the full

incorporation of aerosols in NWP models, aerosol analyses and forecasts from CTMs are rather computationally inexpensive. Thus, the proposed method may be used as an alternative for accounting aerosol impacts in NWP models in the future.

A multitude of options exist for further studying the dynamical downscaling of aerosol fields for incorporation into NWP model forecasts. First, sensitivity studies of WRF-Chem parameterization schemes could be conducted and analyzed for performance. While the indirect aerosol effects can also be investigated, researchers should bear in mind the difficulties associated with proving the smoke plume is the cause of cloud and precipitation changes. Finally, this study can be expanded to include additional smoke plume case studies in a variety of regions as well as additional aerosol event types such as dust events.

REFERENCES

- [1] Ackermann, A. S., O. B. Toon, D. E. Stevens, A. J. Heymsfield, V. Ramanathan, and E. J. Welton, 2000: Reduction of Tropical Cloudiness by Soot. *Sci.*, **288**, 1042-1047, DOI: 10.1126/science.288.5468.1042.
- [2] Ahmadov, R., and Coauthors, 2019: Forecasting smoke, visibility and smoke-weather interactions using a coupled meteorology-chemistry modeling system: Rapid Refresh and High-Resolution Rapid Refresh coupled with Smoke (RAP/HRRR-Smoke). *Geophys. Res. Abs.*, Vol. 21 of, EGU2019-18605, Vienna, Austria <https://meetingorganizer.copernicus.org/EGU2019/EGU2019-18605.pdf> (Accessed March 23, 2020).
- [3] Alfaro-Contreras, R., J. Zhang, J. R. Campbell, and J. S. Reid, 2016: Investigating the frequency and interannual variability in global above-cloud aerosol characteristics with CALIOP and OMI. *Atmos. Chem. Phys.*, **16**, 47–69, <https://doi.org/10.5194/acp-16-47-2016>.
- [4] Baklanov, A., and Coauthors, 2014: Online coupled regional meteorology chemistry models in Europe: current status and prospects. *Atmos. Chem. Phys.*, **14**, 317-398.
- [5] Benedetti, A. and F. Vitart, 2018: Can the Direct Effect of Aerosols Improve Subseasonal Predictability? *Mon. Wea. Rev.*, **146**, 3481-3498, doi: 10.1175/MWR-D-17-0282.1.

- [6] Chen, F., and J. Dudhia, 2001: Coupling an Advanced Land Surface–Hydrology Model with the Penn State–NCAR MM5 Modeling System. Part I: Model Implementation and Sensitivity. *Mon. Wea. Rev.*, **129**, 569–585.
- [7] Chen, S.-H., and W.-Y. Sun, 2002: A One-dimensional Time Dependent Cloud Model. *J. Met. Soc. Japan. Ser. II*, **80**, 99–118, <https://doi.org/10.2151/jmsj.80.99>.
- [8] CIFFC, 2015: On June 29, Canada had total of 1 million hectares burnt. 6 days later, we have just passed 2.1 million hectares. <http://www.ciffc.ca/firewire/current.php>, @CIFFC, <https://twitter.com/CIFFC/status/617794234460979200> (Accessed November 1, 2019).
- [9] Clement, C. F., and I. J. Ford, 1999: Gas-to-particle conversion in the atmosphere: I. Evidence from empirical atmospheric aerosols. *Atmos. Env.*, **33**, 475–487, [https://doi.org/10.1016/S1352-2310\(98\)00264-7](https://doi.org/10.1016/S1352-2310(98)00264-7).
- [10] Cooke, W. F., C. Liousse, H. Cachier, and J. Feichter, 1999: Construction of a 1° x 1° fossil fuel emission data set for carbonaceous aerosol and implementation and radiative impact in the ECHAM4 model. *J. Geophys Res.*, **104**, 22137–22162, doi: 10.1029/1999JD900187.
- [11] Eck, T. F., B. N. Holben, J. S. Reid, O. Dubovik, A. Smirnov, N. T. O’Neill, I. Slutsker, and S. Kinne, 1999: Wavelength dependence of the optical depth of biomass burning, urban, and desert dust aerosols. *J. Geophys. Res. Atmos.*, **104**, 31333–31349, <https://doi.org/10.1029/1999JD900923>.
- [12] Fast, J. D., W. I. Gustafson, R. C. Easter, R. A. Zaveri, J. C. Barnard, E. G. Chapman, G. A. Grell, and S. E. Peckham, 2006: Evolution of ozone, particulates, and aerosol direct radiative forcing in the vicinity of Houston using a

- fully coupled meteorology-chemistry-aerosol model. *J. Geophys. Res. Atmos.*, **111**, <https://doi.org/10.1029/2005JD006721>.
- [13] Feingold, G., H. Jiang, and J. Y. Harrington, 2005: On smoke suppression of clouds in Amazonia. *Geophys. Res. Lett.*, **32**, <http://doi.org/10.10129/2004GL021369>.
- [14] Ginoux, P., M. Chin, I. Tegen, J. M. Prospero, B. Holben, O. Dubovik, and S.-J. Lin, 2001: Sources and distributions of dust aerosols simulated with the GOCART model. *J. Geophys. Res. Atmos.*, **106**, 20255–20273, <https://doi.org/10.1029/2000JD000053>.
- [15] Grell, G. A., S. E. Peckham, R. Schmitz, S. A. McKeen, G. Frost, W. C. Skamarock, and B. Eder, 2005: Fully coupled “on-line” chemistry within the WRF model. *Atmos. Env.*, **39**, 6957–6975, <https://doi.org/10.1016/j.atmosenv.2005.04.027>.
- [16] Herzmann, D., ASOS-AWOS-METAR Data Download. *Iowa Environmental Mesonet*. <https://mesonet.agron.iastate.edu/request/asos/hourlyprecip.phtml> (Accessed June 13, 2019).
- [17] Hogan, T. F. and co-authors, 2014: The Navy Global Environmental Model. *Oceanography*, **27**, 114-125, <http://doi.org/10.5670/oceanog.2014.73>.
- [18] Holben, B. N., and Coauthors, 1998: AERONET—A Federated Instrument Network and Data Archive for Aerosol Characterization. *Rem. Sens. Env.*, **66**, 1–16, [https://doi.org/10.1016/S0034-4257\(98\)00031-5](https://doi.org/10.1016/S0034-4257(98)00031-5).
- [19] Hong, S.-Y., Y. Noh, and J. Dudhia, 2006: A New Vertical Diffusion Package with an Explicit Treatment of Entrainment Processes. *Mon. Wea. Rev.*, **134**, 2318–2341, <https://doi.org/10.1175/MWR3199.1>.

- [20] Iacono, M. J., J. S. Delamere, E. J. Mlawer, M. W. Shephard, S. A. Clough, and W. D. Collins, 2008: Radiative forcing by long-lived greenhouse gases: Calculations with the AER radiative transfer models. *J. Geophys. Res. Atmos.*, **113**, <https://doi.org/10.1029/2008JD009944>.
- [21] IPCC, 2014: Climate Change 2014: *Synthesis Report, Contribution of Working Groups I, II, and III to the Fifth Assessment Report of the Intergovernmental Panel on Climate Change [Core Writing Team, R. K. Pachauri and L. A. Meyer (eds)]*. <https://www.ipcc.ch/report/ar5/syr/> (Accessed October 28, 2019).
- [22] Jin, M., J. M. Shepherd, and W. Zheng, 2010: Urban Surface Temperature Reduction via the Urban Aerosol Direct Effect: A Remote Sensing and WRF Model Sensitivity Study. *Adv. Met.*, <https://doi.org/10.1155/2010/681587>.
- [23] Kahn, R. A., B. J. Gaitley, M. J. Garay, D. J. Diner, T. F. Eck, A. Smirnov, and B. N. Holben, 2010: Multiangle Imaging SpectroRadiometer global aerosol product assessment by comparison with the Aerosol Robotic Network. *J. Geophys. Res.*, **115**, D23209, DOI: 10.1029/2010JD014601.
- [24] Kain, J. S., 2004: The Kain–Fritsch Convective Parameterization: An Update. *J. Appl. Meteor.*, **43**, 170–181.
- [25] Kaufman, Y. J., and I. Koren, 2006: Smoke and Pollution Aerosol Effect on Cloud Cover. *Sci.*, **313**, 655–658, <https://doi.org/10.1126/science.1126232>.
- [26] Koren, I., Y. J. Jaugman, L. A. Remer, and J. V. Martins, 2004: Measurement of the Effect of Amazon Smoke on Inhibition of Cloud Formation. *Sci.*, **303**, 5662, 1342–1345, DOI: 10.1126/science.1089424.

- [27] Lioussé, C., J. E. Penner, C. Chuang, J. J. Walton, H. Eddleman, and H. Cachier, 1996: A global three-dimensional model study of carbonaceous aerosols. *J. Geophys Res.*, **101**, 19411-19432.
- [28] Lynch, P., and Coauthors, 2016: An 11-year global gridded aerosol optical thickness reanalysis (v1.0) for atmospheric and climate sciences. *Geo. Mod. Dev.*, **9**, 1489–1522, <https://doi.org/10.5194/gmd-9-1489-2016>.
- [29] Naval Research Laboratory, 2019: Navy Aerosol Analysis and Prediction System (NAAPS) Global Aerosol Model. Naval Research Laboratory, last accessed 1 March 2019.
- [30] NCEI, Model Datasets — National Centers for Environmental Information (NCEI) formerly known as National Climatic Data Center (NCDC). *National Centers for Environmental Information*,. <https://www.ncdc.noaa.gov/data-access/model-data/model-datasets> (Accessed November 1, 2019).
- [31] NDSU School of Natural Resource Sciences, 2020: North Dakota Agricultural Weather Network (NDAWN) Hourly Weather Data. NDSU School of Natural Resource Sciences, accessed 22 July 2020, <http://ndawn.ndsu.nodak.edu/weather-data-hourly.html>.
- [32] Peckham, S., and Coauthors, 2011: WRF-Chem Version 3.3 User’s Guide.
- [33] Powers, J. G., and Coauthors, 2017: The Weather Research and Forecasting Model: Overview, System Efforts, and Future Directions. *Bull. Amer. Meteor. Soc.*, **98**, 1717–1737, <https://doi.org/10.1175/BAMS-D-15-00308.1>.
- [34] Pryor, S. C., P. Crippa, and R. C. Sullivan, 2015: Atmospheric Chemistry. *Reference Module in Earth Systems and Environmental Sciences*, Elsevier.

- [35] Research Data Archive at the National Center for Atmospheric Research, Computational and Information Systems Laboratory, 2015: NCEP North American Mesoscale (NAM) 12 km Analysis. RDA at the NCAR, Computational and Information Systems Laboratory, last accessed 2 July 2019, <https://doi.org/10.5065/G4RC-1N91>.
- [36] Robock, A., 1991: Surface cooling due to forest fire smoke. *J. Geo. Res.*, **96**, 20869-20878, <https://doi.org/10.1029/91JD02043>.
- [37] Schmid, P., and D. Niyogi, 2012: A Method for Estimating Planetary Boundary Layer Heights and Its Application over the ARM Southern Great Plains Site. *J. Atmos. Oceanic Technol.*, **29**, 316–322, <https://doi.org/10.1175/JTECH-D-11-00118.1>.
- [38] Shi, Y., J. Zhang, J. S. Reid, B. Liu, and E. J. Hyer, 2014: Critical evaluation of cloud contamination in the MISR aerosol products using MODIS cloud mask products. *Atmos. Meas. Tech.*, **7**, 1791-1801, <https://doi.org/10.5194/amt-7-1791-2014>.
- [39] Skamarock, C., and Coauthors, 2008: A Description of the Advanced Research WRF Version 3. NCAR Tech. Note NCAR/TN-475+STR, 113 pp, <https://doi.org/10.5065/D68S4MVH>.
- [40] Stull, R. B., *An Introduction to Boundary Layer Meteorology*. Kluwer Academic Publishers, 666 pp.
- [41] UCAR: WRF-Chem Version 3.9.1.1 User’s Guide.
- [42] Walters, D., and Coauthors, 2019: The Met Office Unified Model Global Atmosphere 7.0/7.1 and JULES Global Land 7.0 configurations. *Geo. Mod. Dev.*, **12**, 1909–1963, <https://doi.org/10.5194/gmd-12-1909-2019>.

- [43] Westphal, D. and O. B. Toon, 1991: Simulations of microphysical, radiative, and dynamical processes in a continental-scale forest fire smoke plume. *J. Geophys. Res. Atmos.*, **96**, 22379-22400, <https://doi.org/10.1029/91JD01956>.
- [44] Yorks, J. E., M. J. McGill, V. S. Scott, S. W. Wake, A. Kupchock, D. L. Hlavka, W. D. Hart, and P. A. Selmer, 2014: The Airborne Cloud–Aerosol Transport System: Overview and Description of the Instrument and Retrieval Algorithms. *J. Atmos. Oceanic Technol.*, **31**, 2482–2497, <https://doi.org/10.1175/JTECH-D-14-00044.1>.
- [45] Zhang, J., J. S. Reid, D. L. Westphal, N. L. Baker, E. J. Hyer, 2008: A system for operational aerosol optical depth data assimilation over global oceans. *J. Geophys. Res.*, **113**, doi: 10.1029/2007JD009065.
- [46] Zhang, J., J. S. Reid, M. Christensen, and A. Benedetti, 2016: An evaluation of the impact of aerosol particles on weather forecasts from a biomass burning event over the Midwestern United States: observational-based analysis of surface temperature. *Atmos. Chem. Phys.*, **16**, 6475-6494, <http://doi.org/10.5194/acp-16-6475-2016>.
- [47] Zhang, Y., 2008: Online-coupled meteorology and chemistry models: history, current status, and outlook. *Atmos. Chem. Phys.*, **8**, 2895-2932, <https://doi.org/10.5194/acp-8-2895-2008>.

